THE JOURNAL OF PHYSICAL CHEMISTRY B
A JOURNAL OF THE AMERICAN CHEMICAL SOCIETY

pubs.acs.org/JPCB

Article

Complex Formation and Dissociation Dynamics on Amorphous Silica Surfaces

Published as part of The Journal of Physical Chemistry virtual special issue "W. E. Moerner Festschrift".

Steven A. Yamada, Samantha T. Hung, Jae Yoon Shin, and Michael D. Fayer*

Cite This: *J. Phys. Chem. B* 2021, 125, 4566–4581

Read Online

ACCESS | Metrics & More | Article Recommendations | Supporting Information

ABSTRACT: Benzene complex formation and dissociation dynamics with silanols on the amorphous silica surfaces of nanoporous SiO_2, from a benzene/carbon tetrachloride solution, were measured by the growth of off-diagonal peaks in the two-dimensional infrared (2D IR) chemical exchange spectrum of the isolated Si−OD stretch. The presence of two types of isolated silanols, termed type I and II, was revealed, with dissociation time constants of 82 and 4.0 ps, respectively. The type I silanols are associated with the main IR absorption feature in the Si−OD stretching region, while the type II silanols give rise to a broader shoulder to lower frequency. Polarization selective pump−probe (PSPP) measurements provided the vibrational lifetimes and orientational relaxation rates of the two silanols in the CCl_4 (free) and benzene (complex) environments. The type II silanols constitute roughly 30% of the isolated silanol population and exhibit a substantially faster rate of vibrational relaxation, making the type I dynamics the dominant contribution to the PSPP and 2D IR signals. From the measured dissociation times, the enthalpies of formation for the two surface complexes were obtained, with the formation of the type I complex being significantly more exothermic. As the type II site is preferentially removed from the amorphous silica surface with increasing activation temperature, the results provide a reasonable explanation for the increased exothermicity of benzene adsorption on silica with increasing activation temperature in previous calorimetry experiments.

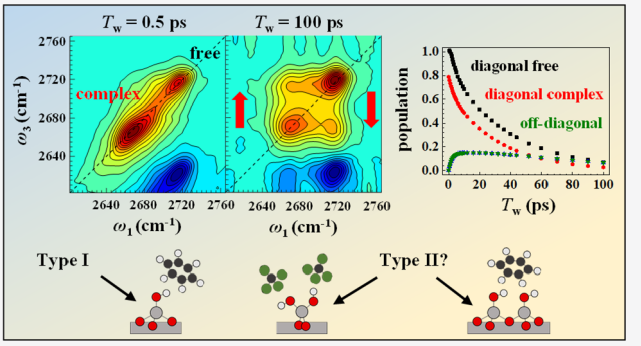

I. INTRODUCTION

Amorphous silica (SiO_2) surfaces have become increasingly important in areas such as catalysis, chemical separations, adsorption,[1−3] and macromolecule folding.[4] However, the task of predicting the effects of amorphous SiO_2 surfaces in new applications and devices remains challenging. This reflects the incomplete nature of current models and the need for further experimental studies of molecular scale surface structures and dynamics.

Broadly speaking, the amorphous silica surface can be separated into regions, or domains, that are relatively hydrophobic or hydrophilic.[5,6] The sizes, shapes, and distributions of these domains are irregular and have proven challenging to model.[7,8] Whether a region is less or more hydrophilic depends on its content of siloxane (Si−O−Si) and silanol (Si−OH) groups, respectively. Silanols can be divided into those forming hydrogen-bonds (H-bonds) with other surface groups and those that do not. Silanols that do not form H-bonds can be further subdivided into isolated (Q3), vicinal (Q3), and geminal (Q2) silanols (Figure 1), where the number accompanying the letter "Q" denotes the number of surface O atoms directly bonded to the Si atom.[4,9] Isolated and vicinal silanols both have one OH per Si atom, but vicinal silanols are further distinguished by the fact that they share a common O atom (and thus come in pairs).[4] Geminal silanols are unique in having two OH groups bonded to a single Si atom.[4,9]

Experimentally, it is possible to distinguish between Q2, Q3, and Q4 (Si atoms coordinated to four oxygen atoms) Si atoms, which produce distinct peaks in ^{29}Si cross-polarization/magic angle spinning NMR spectra.[10−12] However, it appears that no single method can effectively discriminate between isolated and vicinal Q3 silanols. To complicate matters, the number and type of surface silanols are strongly dependent on the temperature of activation used to prepare the samples.[9] These challenges have led to discrepancies in IR absorption band assignments[13,14] and varying conclusions on the surface composition by different authors, particularly with respect to the question of whether vicinal silanols exist above ~400 °C.[9,14]

Received: February 9, 2021
Revised: March 30, 2021
Published: April 23, 2021

https://doi.org/10.1021/acs.jpcb.1c01225
J. Phys. Chem. B 2021, 125, 4566−4581

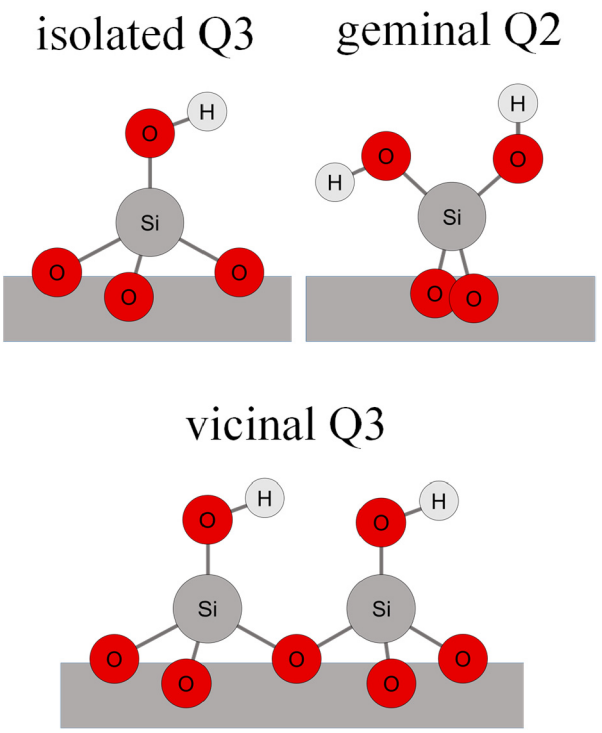

Figure 1. Illustration of the three main types of isolated silanols: isolated Q3, geminal Q2, and vicinal Q3. The number following the letter "Q" indicates the number of surface O atoms coordinated to the silanol Si atom.

Additionally, the amorphous silica surface exhibits variations in nanotopography as revealed by methods such as AFM.[15] The surface roughness and presence of cavities can affect the accessibility and affinity of silanols to interfacial molecules by perturbing their electronic structure.[16] *Ab initio* molecular dynamics (MD) simulations also indicate that the local surface environment can impact the pK_a of silanols, for example, by stabilizing the silanolate base.[16,17] The structure of the silanols and their surroundings may need to be considered simultaneously to rationalize the well-known bimodal acidity of the silica surface, which features pK_a values of 8.5 and 4.5 in a ratio of 4:1.[18] However, the molecular origin of these two acidities remains unclear and is an active area of study.[16,17,19,20]

Here, the reversible adsorption of an H-bond acceptor molecule on isolated surface silanols in the pores of nanoporous silica is probed with 2D IR chemical exchange spectroscopy.[21−23] Surface adsorption is a basic process that is fundamental to applications of amorphous silica surfaces. In this study, the term "isolated" will be used in a general sense to refer to all silanols that are sufficiently separated to not interact with other silanols, which can include isolated Q3, vicinal Q3, and geminal Q2 silanols. In the event that we need to distinguish between truly isolated silanols from vicinals and geminals, we will refer to them as isolated Q3 silanols.

The sample under investigation was a deuterated mesoporous silica, MCM-41, filled with a benzene/carbon tetrachloride mixture. The OD stretching vibrational mode of the isolated silanols was used as a local probe of the surface environment and to monitor the reversible formation of benzene surface complexes, which red-shifts the absorption enough that the complex and free sites are spectrally distinct. Polarization selective pump−probe (PSPP) experiments on MCM-41 in the pure solvents revealed two rates of vibrational relaxation that were attributed to two types (I and II) of isolated silanols in different structural environments. The longer lifetime component (I) gives rise to the main absorption feature in the isolated Si−OD stretching region and was assigned to isolated Q3 silanols. The anisotropy decays obtained from the PSPP measurements approached a plateau in either pure solvent, demonstrating that the rotational motion is sterically hindered, although to a lesser extent compared to other surface bound OD groups.[24]

2D IR experiments on the mixed solvent revealed the time-dependent growth of off-diagonal chemical exchange peaks. Analysis of the spectra revealed that the off-diagonal peaks experienced an initial rapid growth that was sustained by a much slower growth process that became dominant on longer time scales. By use of a two-site chemical exchange model, the spectra were decomposed into contributions from type I and II silanols, which were found to be responsible for the slow and fast growths, respectively. The standard enthalpies of formation obtained from the complex dissociation times for the two sites were in reasonable quantitative agreement with calorimetry measurements of benzene adsorption on silica gel and qualitatively agree with the two-site thermodynamic trends for crystal violet cation adsorption on silica.[25,26] The structural nature of the type II silanol is discussed in the context of these studies.

II. EXPERIMENTAL PROCEDURES

II.A. Deuteration of Surface Silanols. Studying the Si−OD, as opposed to the Si−OH, stretching mode is experimentally advantageous because the lower frequency of the Si−OD vibration better matches with the operating frequency range of our 2D IR spectrometer, which is determined by many factors including phase-matching conditions, optical transmission windows, and grating efficiencies. In addition, as discussed below, the results found here are compared to experiments on triethylsilanol-OD in benzene/CCl_4 bulk solutions.

The MCM41 and deuterium oxide (D_2O) at 99.8% purity were purchased from ACS Material and CortecNet, respectively. The specific BET surface area[27] (950 ± 70 m^2/g), pore size distribution[28] (mean ± SD = 2.8 ± 0.1 nm), and primary mesopore volume[29,30] of the MCM41 (0.75 ± 0.06 cm^3/g) were previously determined.[31]

Several grams of the MCM41 was loaded into a three-necked round-bottom flask (rbf). One of the outer necks was left unused and sealed off with a glass pennyhead stopper and vacuum grease. The opposing outer neck was sealed with a rubber septum. The central neck was attached to a Schlenk line held at a pressure of 100 mTorr by way of a glass adapter with an adjustable stopcock. To remove adsorbed water from the MCM41 pores, the rbf was opened to the Schlenk line and heated to 200 °C overnight. Once the pressure in the line re-equilibrated to 100 mTorr, the rbf was closed from the line and allowed to cool to room temperature (RT). Once cooled, 5 g of D_2O was injected through the rubber septum into the rbf. After 10 min, the rbf was reopened to the Schlenk line and gradually brought back to a temperature of 200 °C to remove the D_2O and redry the MCM41. Once the pressure reading returned to 100 mTorr, the D_2O injection and drying processes were repeated two more times for a total of three times. The dry, deuterated MCM41 (MCM41-OD) was transferred to a N_2(g) glovebox and stored in an airtight scintillation vial for later use.

https://doi.org/10.1021/acs.jpcb.1c01225
J. Phys. Chem. B 2021, 125, 4566−4581

II.B. Sample Preparation. All samples were prepared under an inert atmosphere of a N_2(g) glovebox. MCM41-OD powder was placed in the center of a 56 μm thick, 8 mm inner (13 mm outer) diameter polytetrafluoroethylene (PTFE) spacer centered on top of a 3 mm thick, 25.4 mm diameter CaF_2 window. A second, 25.4 mm outer diameter, 56 μm thick PTFE spacer was placed and centered on top of the window. Anhydrous benzene (Bz) and carbon tetrachloride (CCl_4), purchased from Sigma-Aldrich were mixed in a molar ratio of 1:5, respectively. While a second CaF_2 window was lowered on top of the first, the Bz/CCl_4 solution was pipetted in-between the two windows to completely submerge the MCM41-OD powder as well as fill the gap between the two PTFE spacers. The two CaF_2 windows were held together in a custom-designed aluminum sample cell. To further protect the sample from atmospheric water, isotopic exchange, and solvent evaporation, the sample cell was submerged in liquid Parowax at 60 °C. The cell was then removed, and the wax was allowed to solidify. During this process, masking tape was placed over the portion of the cell that normally exposes the CaF_2 windows to prevent them from being covered in wax. The tape was removed after the wax solidified. Samples of the bulk solvents Bz, CCl_4, and 1:5 Bz:CCl_4 were prepared in the same manner as described above with the exclusion of the smaller PTFE spacer.

II.C. Optical Methods. The laser system and optical setup,[32] FT IR,[33] PSPP,[34] and 2D IR experiments[35−37] have been discussed in detail previously. Descriptions of both the equipment and the experimental techniques are given in the Supporting Information.

III. RESULTS AND DISCUSSION

III.A. Linear Absorption of Isolated Silanols. Figure 2 displays the background-subtracted spectra in the OD stretch region of MCM41-OD activated under vacuum at 200 °C and filled with CCl_4 (green curve), Bz (red curve), and 1:5 Bz:CCl_4 (black curve). When the MCM41-OD is filled with CCl_4, no H-bond can be formed between the surface silanols and the solvent.

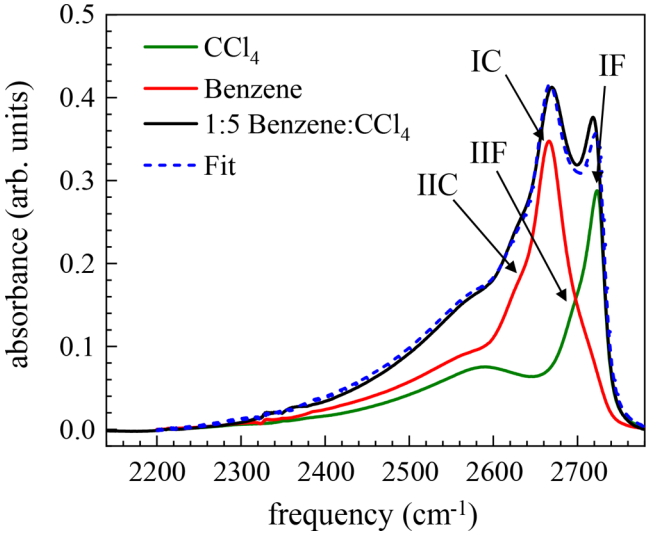

Figure 2. Background subtracted linear absorption spectra of silanol groups on the amorphous silica surface of MCM-41 in the Si−OD stretching region with the pores filled with CCl_4 (green curve), benzene (red curve), and 1:5 benzene:CCl_4 (black curve). The dashed blue curve is the linear combination of pure solvent spectra that provides the best fit to the mixed solvent spectrum.

The sharp peak corresponding to isolated Q3 silanols is located at 2723 cm^{-1}, and the broad, H-bond donor silanol band is observed at 2590 cm^{-1}. The peak at 2723 cm^{-1} is clearly asymmetric with an obvious shoulder on the lower frequency side. This shoulder is highly suggestive of a second silanol species that may be structurally distinct from the isolated Q3 type.

McFarlan and Morrow analyzed the isolated silanol peak as a function of temperature in aerosil silica and precipitated silica initially vacuum activated at 450 °C.[14] They found that when the silica is cooled to −191 °C from 22 °C, the peak broadens. They surmised that the isolated silanol peak is actually a composite of two peaks whose separation increases with decreasing temperature. They further observed that the asymmetric peak at 2760 cm^{-1} and 22 °C (in the deuterated silicas) splits into a doublet with a main peak at 2762.7 cm^{-1} and a shoulder at 2756 cm^{-1} when cooled to −191 °C. We also observe clear evidence of a main peak and shoulder in MCM41-OD filled with CCl_4 at RT (Figure 2). The shoulder was not obvious at 22 °C in the dry silicas investigated by the above authors. Our result suggests that this peak is indeed composed of two peaks that experience a differential solvatochromic shift when immersed in the CCl_4 solvent.

The main peak in MCM41-OD filled with Bz red-shifts to 2666 cm^{-1} and noticeably broadens with respect to the CCl_4 sample. This constitutes a frequency shift of 57 cm^{-1}, which can be attributed to the formation of a π H-bond complex between Bz and the silanol groups on the surface.[24,38,39] Despite the increase in width, the lower frequency shoulder is still clearly observed, showing that this feature is conserved across solvents of differing interaction strengths. A peculiar feature of the Bz spectrum is the presence of a second more subtle shoulder to the blue of the main peak at 2666 cm^{-1}. This shoulder appears to roughly coincide in frequency with the main peak at 2723 cm^{-1} in the CCl_4 sample. It may arise from a small portion of the isolated Q3 silanols that can only very weakly interact with the Bz solvent. This might be the case for silanols embedded in a cavity within the surface. For these sites, the Bz may not be able to orient itself in a manner for its π-electron system to optimally accept an H-bond from the Si−OD donor.

When the silica pores are filled with a binary mixture of 1:5 Bz:CCl_4, both of the main peaks corresponding to isolated Q3 silanols in the two environments are observed. However, the benzene and CCl_4 associated peak maxima are blue-shifted by ~3 cm^{-1} and red-shifted by ~5 cm^{-1}, respectively (Table 1).

Table 1. Parameters for Isolated Silanol OD Stretch Line Shapes

solvent	center(s) (cm^{-1})	fwhm (cm^{-1})
Bz	2666.2 ± 0.2	68 ± 1
CCl_4	2723.4 ± 0.1	38.5 ± 0.7
1:5 Bz:CCl_4	2669.2 ± 0.2	
	2718.2 ± 0.2	

The red shoulder arising from the second type of silanol complexed with Bz can still be observed in the mixed spectrum, but the analogous CCl_4 peak is obscured by the spectral overlap. From this point, we will refer to the Bz and CCl_4 associated silanol peaks in the mixed solvent system as the complex (C) and free (F) peaks, respectively. The isolated Q3 silanols and the second population of silanols will be termed type I and type II,

https://doi.org/10.1021/acs.jpcb.1c01225
J. Phys. Chem. B 2021, 125, 4566−4581

respectively. Thus, a total of four possible surface sites exist in the solvent mixture: IC, IF, IIC, and IIF.

Figure 2 indicates that both the C and F species are present when a binary mixture of Bz and CCl_4 is confined in the MCM41-OD pores (black curve). At room temperature, the C and F forms are likely not static, but under a state of dynamic equilibrium. However, if site II is structurally different from site I, this imposes an additional constraint on the pathways of interconversion. More specifically, the I and II forms, being structurally distinct and physically distant from each other on the surface, cannot interconvert. This means that dynamic equilibrium is independently maintained between IF ↔ IC and IIF ↔ IIC only. In either case, we require the equilibrium constant of the following phase-exchange reaction:

$$F + Bz \rightleftharpoons C + CCl_4 \tag{1}$$

where F and C respectively represent the free (Si−OD···CCl_4) and complex (Si−OD···Bz) silanol forms on the silica surface. Previously, Thomas and Eon measured the adsorption isotherm of Bz on a silica gel from Bz/CCl_4 binary solutions.[40] They concluded that the system behavior could be reasonably accounted for by a monolayer model of the type derived by Everett.[41,42] In the ideal case, Everett considers the surface and binary solution with which it is in direct contact as a series of stacked lattice planes. Note that in the case of MCM41 with a cylindrical pore structure the layers are more appropriately described as lattice rings rather than planes. He further assumed the adsorption to be monomolecular, with the mole fractions (x_i) of the two components constant in all planes except the one in direct contact with the surface; the mole fractions in this plane differing from all other liquid planes because of preferential adsorption of one of the components. With these assumptions, Everett derived the constant[41]

$$K' = \frac{x_C x_{CCl_4}}{x_F x_{Bz}} \tag{2}$$

where $x_F = n_F/(n_F + n_C)$, $x_C = n_C/(n_F + n_C)$, $x_{CCl_4} = n_{CCl_4}/(n_{CCl_4} + n_{Bz})$, and $x_{Bz} = n_{Bz}/(n_{CCl_4} + n_{Bz})$; n_i is the number of moles of species i. Here, x_{CCl_4} and x_{Bz} are also constants because the number of molecules involved in the surface complexation is negligible compared to the number of molecules in the pores. Therefore, a new equilibrium constant can be defined:

$$K_{eq} \equiv \frac{K' x_{Bz}}{x_{CCl_4}} = \frac{x_C}{x_F} \tag{3}$$

The equilibrium constant, K_{eq}, is associated with the simplified dynamic equilibrium, F ⇌ C, that describes the present measurements. Clearly, if the Bz:CCl_4 ratio is increased, a greater number of complex relative to free silanols will form, leading to an increased K_{eq}. Note that the single concentration studied here (1:5 Bz:CCl_4) was chosen because it produced comparable signal levels from the free and complexed silanol populations. In this context, eq 3 is more useful than eq 2 because the IR observables are only sensitive to the surface silanol populations.

The 1:5 Bz:CCl_4 spectrum (black curve, Figure 2), A, can be described by $A = x_C A_C + x_F A_F$, where A_C and A_F are the spectra with all of the isolated silanols associated with pure Bz or pure CCl_4. The effective equilibrium constant for the isolated silanols (eq 3) can be estimated by fitting the 1:5 Bz:CCl_4 spectrum with a linear combination of the Bz and CCl_4 spectra. The resulting fit is also shown in Figure 2 (dashed, blue curve). Note that the Bz and CCl_4 spectra actually presented in Figure 2 are equal to the original spectra, A_C and A_F, multiplied respectively by the factors $x_C = 0.31$ and $x_F = 0.55$ obtained from the fit. The sum of these spectra is equal to the fit curve. The spectrum of the mixture is plotted in the original OD units of absorbance. From eq 3, the resulting equilibrium constant is $K_{eq} \sim 0.6$.

Considering the rather involved assembly procedure required for these powdered samples, it is likely that there is some deviation in path length from sample to sample. Such a fitting procedure relies on the path length remaining fixed across the samples so that any variation in absorbance can be attributed to a change in mole fraction of the absorbing species. We estimate the errors on the mole fractions x_C and x_F to be on the order of 0.1 and the error on K_{eq} determined in this manner to be about 0.2. Also note that an implicit assumption of the fitting is that the transition dipole moment (extinction coefficient) in a given local solvent environment (e.g., Si−OD···CCl_4 or Si−OD···Bz) is independent of whether the liquid phase is a pure solvent or the mixture solution. In section III.D, K_{eq} will be independently determined in a model fit to the 2D IR spectra for the mixed solvent system. The value obtained, $K_{eq} = 0.8 \pm 0.1$, is in reasonable agreement with the estimate of 0.6 obtained from the linear absorption spectra alone.

III.B. Vibrational Relaxation of the Si−OD Stretching Mode. To further elucidate the properties of the silanol populations, we measured the vibrational lifetime of the isolated Si−OD stretch band in CCl_4 and Bz. The isotropic data, $P(t)$, which is the vibrational population relaxation, was obtained from the experimental PSPP signals, $S_{\parallel}(t)$ and $S_{\perp}(t)$ (see the Supporting Information). $S_{\parallel}(t)$ and $S_{\perp}(t)$ are the pump−probe signals observed with the probe pulse signal having polarization parallel to and perpendicular to the pump polarization, respectively.

$$P(t) = \frac{1}{3}[S_{\parallel}(t) + 2S_{\perp}(t)] \tag{4}$$

Figure 3 displays the $P(t)$ signals as a function of frequency for the OD stretch 0−1 transition in (a) CCl_4 and (b) Bz. Note that an undesired heating signal,[43,44] which produced a frequency dependent offset at long time delays, was removed from $P(t)$ as described in the Supporting Information. Removal of the small heating contribution to the signal from $S_{\parallel}(t)$ and $S_{\perp}(t)$ yields the correct $P(t)$ and $r(t)$, the orientational anisotropy discussed below.

The heat-subtracted $P(t)$ signals in Figure 3 (solid points) are discernibly biexponential for both solvents and can be fit (solid curves) to a function of the form $P(t) = A_{II}e^{-t/T_1^{II}} + A_I e^{-t/T_1^{I}}$, where II and I refer to the silanol type, discussed further below. For either solvent, the decays can be described with two frequency-independent lifetimes: T_1^{II} and T_1^{I}. Only the amplitudes, A_{II} and A_I, of the lifetime components vary with frequency. The two lifetimes are $T_1^{II} = 17.8 \pm 0.8$ ps and $T_1^{I} = 71 \pm 2$ ps in CCl_4 and $T_1^{II} = 15 \pm 1$ ps and $T_1^{I} = 46.7 \pm 0.6$ ps in Bz. The presence of two distinct lifetimes in each solvent is consistent with the observation of two bands in the linear absorption spectra of Figure 2. For comparison, only a single lifetime was measured for deuterated triethylsilanol (TES) in bulk CCl_4 (160 ps) and Bz (95 ps).[45] Also note that the longer surface Si−OD lifetime, T_1^{I}, is very sensitive to the solvent and decreases by ∼35% when the solvent is changed from CCl_4 to

https://doi.org/10.1021/acs.jpcb.1c01225
J. Phys. Chem. B 2021, 125, 4566−4581

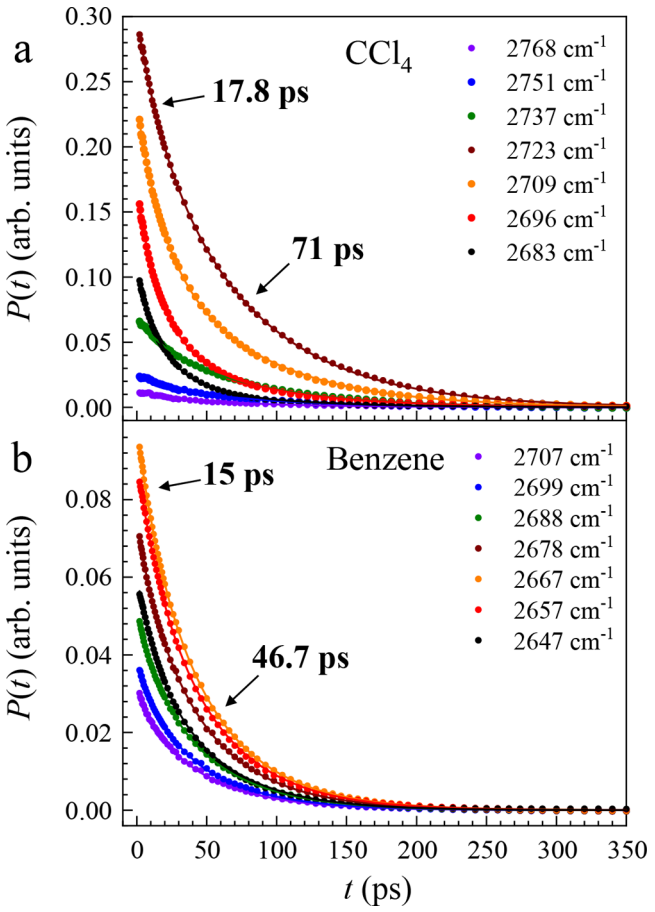

Figure 3. Frequency-dependent isotropic pump−probe signals, $P(t)$, in the isolated Si−OD stretching region for silanols in (a) CCl_4 and (b) benzene in the pores.

Bz. This is similar to the behavior of the single TES lifetime, which decreases by ∼40% between these same solvents.

When the excited vibration ($\nu = 1$) relaxes to the ground state ($\nu = 0$), the energy is transferred to various accepting modes of the system.[46−48] The rate of energy transfer is primarily determined by the number of modes required to conserve energy with the Si−OD stretch vibration and its coupling strength to each accepting mode.[47] In the case of surface silanols and no solvent, the most plausible dissipation pathway involves energy flow into the modes of the SiO_4D tetrahedron and broader silica framework.[46−48] Because the highest vibrational frequencies in bulk silica are under 1200 cm^{-1}, the relaxation likely requires the simultaneous excitation of multiple accepting modes.[47]

Previously, it was found that CCl_4 slightly decreases the vibrational lifetime of silica bound SiOH relative to the same system in vacuum.[46,48] It was proposed that CCl_4−OH collisions mainly enhance the energy transfer rate from the SiOH into the silica framework, whereas energy transfer into the degrees of freedom of the colliding CCl_4 partner was thought to be negligible.[46] This idea is consistent with the transparency of CCl_4 in the SiOH (and Si−OD) stretching region of the IR spectrum.[48] On the other hand, Bz significantly accelerates the surface Si−OD lifetime. Unlike CCl_4, Bz has several combination bands that overlap with the isolated surface Si−OD stretch, for example, a band at ∼2653 cm^{-1} that arises from the combination of in-plane ring modes, $\nu 9 + \nu 19$.[49] Thus, Bz introduces additional pathways for the energy to relax. Additionally, it is well-known that Bz can form an Si−OD···π H-bond at silanol sites on the silica surface.[4,38,39] In their DFT study, Rimola et al. found that the Bz ring lies relatively flat on a model hydroxylated silica surface, with the center of the ring roughly aligned with the hydroxyl.[39] The Si−OD···π interaction favors a short distance between Bz and the silanol, which could

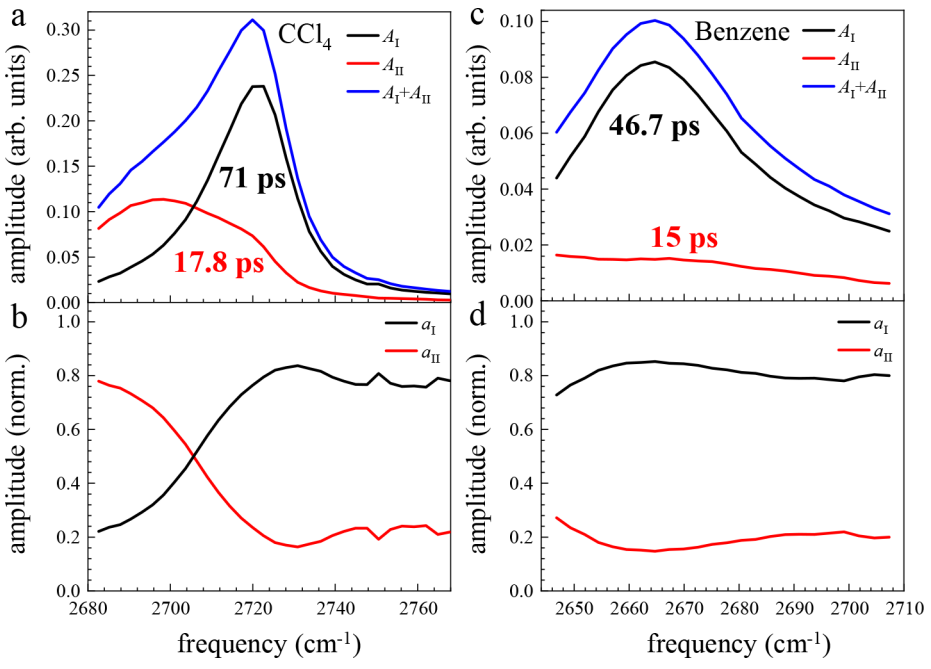

Figure 4. (a) Isotropic pump−probe $t = 0$ spectrum (blue curve) with CCl_4 in the pores, decomposed into its amplitude contributions from type I (A_I, black curve) and type II (A_{II}, red curve) silanols. (b) Frequency-dependent, normalized amplitude contributions from type I (a_I, black curve) and type II (a_{II}, red curve) silanols. (c, d) Same as (a, b) but for benzene in the pores.

https://doi.org/10.1021/acs.jpcb.1c01225
J. Phys. Chem. B 2021, 125, 4566−4581

increase the coupling between the Si−OD stretch and the accepting modes of the solvent.

To our knowledge, the observation of a second, much shorter lifetime component, T_1^{II}, associated with isolated silanols is a new finding. It is not surprising that this <20 ps component was not detected in previous transient absorption studies, which used quite broad ∼14−20 ps pulses.[46−48] The pulse durations used in the present work were 200 fs, or 2 orders of magnitude shorter. Interestingly, the T_1^{II} lifetime is effectively insensitive to the nature of the solvent, decreasing by only 1−2 ps, within error, in Bz relative to CCl_4. This may be an indication that the interaction of Bz with this silanol species is relatively weak.

To understand the origin of the two lifetimes, their amplitudes are plotted as a function of frequency for CCl_4 and Bz in Figures 4a and 4c, respectively. Note that the sum of the two amplitudes can be interpreted as the isotropic transient absorption spectrum at $t = 0$ (before any vibrational relaxation occurs). In the CCl_4 spectrum of Figure 4a, it is clear that two overlapping bands reside underneath the total spectrum (blue curve). The amplitude of the longer lifetime, T_1^I, traces out a relatively narrow and symmetric peak centered at ∼2721 cm^{-1} (black curve) that is responsible for the main feature in the total spectrum. We therefore assign the T_1^I lifetime to isolated Q3 silanols, which we and others[14] have termed type I. In the case of the shorter lifetime, T_1^{II}, the amplitude outlines a broader, less intense peak at ∼2698 cm^{-1} that gives rise to the red shoulder in the total spectrum. Thus, T_1^{II} is associated with the type II silanol discussed in section III.A. In the Bz spectrum (Figure 4c), the intensity exhibits a gradually increasing trend to lower frequencies, although interference from the negative going 1−2 transition signal precludes accurate spectral decomposition for lower frequencies. Consequently, any peak associated with T_1^{II} was not clearly resolved.

If we assume that for a single solvent I and II have the same transition dipole strength, then the amplitudes at fixed frequency provide the relative populations of the two species. In Figures 4b and 4d, the normalized amplitudes, $a_I = A_I/(A_I + A_{II})$ (black curve) and $a_{II} = A_{II}/(A_I + A_{II})$ (red curve), are displayed for CCl_4 and Bz, respectively. The type I silanols comprise ∼80% of the signal around the maximum and to the blue side of the total spectrum. However, the situation reverses to the red side of the spectrum. This is particularly clear in the CCl_4 sample, where the type II silanols comprise ∼80% of the signal.

To summarize, the isotropic PSPP signals revealed the presence of two frequency-independent vibrational lifetimes for the silanols in pure CCl_4 and pure benzene. The short and long lifetime components, in either solvent, can be attributed to type II and type I (isolated Q3) silanols, respectively, by comparing their transient absorption spectra to the linear absorption spectra in Figure 2 and to previous measurements.

III.C. Orientational Relaxation of Isolated Silanols. To analyze the orientational relaxation of the surface silanols, the anisotropic part of the PSPP signals was calculated via[34]

$$r(t) = \frac{S_{\parallel}(t) - S_{\perp}(t)}{S_{\parallel}(t) + 2S_{\perp}(t)} = 0.4C_2(t) \quad (5)$$

where $r(t)$ is the anisotropy and $C_2(t)$ is the orientational correlation function. The orientational correlation function is given by $C_2(t) = \langle P_2(\hat{\boldsymbol{\mu}}(t)\cdot\hat{\boldsymbol{\mu}}(0))\rangle$, where P_2 is the second-order Legendre polynomial, $\hat{\boldsymbol{\mu}}(t)$ is the transition dipole moment unit vector at time t, and $\langle\cdots\rangle$ represents an isotropic ensemble average.[50,51]

The anisotropy for isolated silanols interacting with CCl_4 and Bz is shown as a function of detection frequency in Figures 5a and 5b, respectively. In principle, $r(0) = 0.4$; however, given the finite pulse durations (200 fs), it is not possible to resolve the ultrafast inertial dynamics which occur on a time scale of <100 fs in many liquid phase systems.[52,53] Consequently, $r(0)$ appears to begin below 0.4. The fraction of the decay that is caused by inertial motion can be quantified by the deviation from 0.4. A second key aspect of the decays in Figure 5 is that they approach a nonzero offset (∼0.1) at long time. This indicates that the Si−OD orientation does not completely randomize. However, the Si−OD does rotate to a much greater extent relative to other surface OD groups. For example, the μ_2-OD of the metal−organic framework MIL53(Al) approaches an offset of no less than ∼0.36 when submerged in Bz.[24] The ability of the silanols to sample a larger range of orientations may be attributable not only to rotation about the Si−O bond axis but also to the flexibility of the Si−O−Si linkages that tether them to the surface, permitting out-of-plane motions of the OD (note that one of the Si atoms is directly bonded to the OD). Si−O−Si bonds have quite low angle bending energy barriers, estimated to be ∼0.4−1 kcal/mol for angle deformations of 20°−30° about the equilibrium bond angle in disiloxane.[6,54,55] The Si−O−D

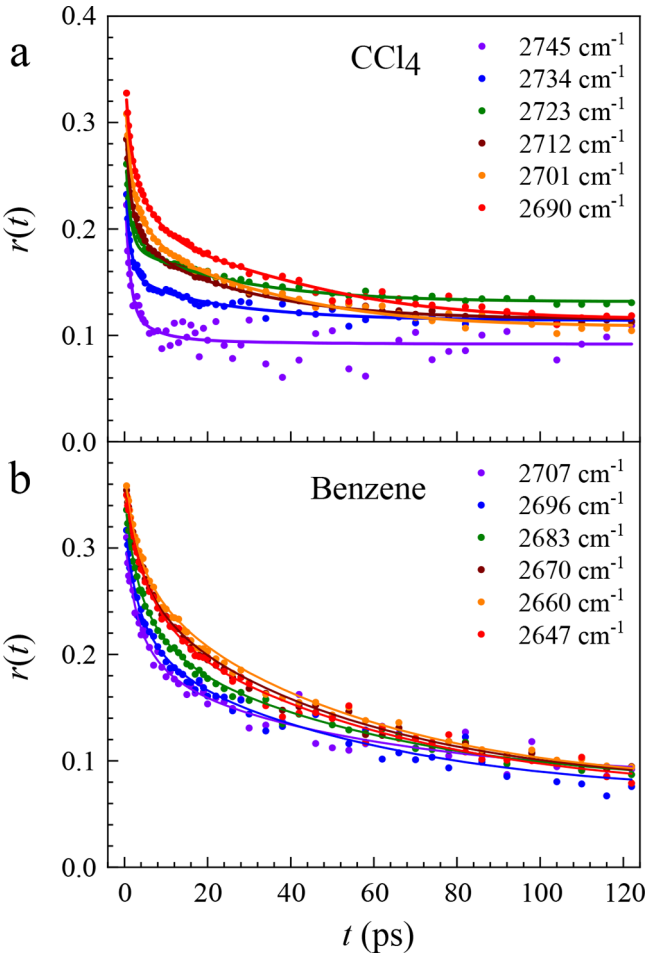

Figure 5. Frequency-dependent reorientational anisotropy data, $r(t)$, in the isolated Si−OD stretching region for silanols with (a) CCl_4 and (b) benzene in the pores. The solid curves in (a) and (b) are respectively two- and one-component fits of a wobbling-in-a-cone model to the data as described in the main text.

https://doi.org/10.1021/acs.jpcb.1c01225
J. Phys. Chem. B 2021, 125, 4566−4581

Table 2. Wobbling-in-a-Cone Model Parameters for Isolated Silanols

silanol	solvent	freq (cm^{-1})	θ_{in} (deg)	θ_{c1} (deg)	θ_{c2} (deg)	τ_{c1} (ps)	τ_{c2} (ps)
II	CCl_4	2698	19 ± 2	28 ± 2	NA	6.5 ± 0.2	
I	CCl_4	2720	28.0 ± 0.5	39 ± 2	NA	1.0 ± 0.1	
II and I	Bz	2670	13.9 ± 0.6	27.9 ± 0.6	48.5 ± 0.6	4.4 ± 0.1	50 ± 1

bond angle may also fluctuate to some degree. While the orientational dynamics of μ_2-OD were found to be relatively insensitive across a range of solvents with varying H-bond acceptor strengths,[24] the Si−OD is affected by the nature of the solvent as seen in Figure 5.

It has been shown that the restricted motion of molecules bound to surfaces can be described as wobbling (diffusion) in a cone of half-angle θ_c.[56−58] The correlation function associated with one diffusive cone is given by $C_2(t) = Q^2 + (1 - Q^2)\exp[-t/\tau_c]$, where τ_c is the orientational correlation time for restricted angular diffusion and Q^2 is the square of a generalized order parameter, $Q^2 = [0.5\cos\theta_c(1 + \cos\theta_c)]^2$. The limiting value of the anisotropy at long time is given by $r(\infty) = 0.4Q^2$, providing a direct relationship between θ_c and the anisotropy plateau. More restricted environments are characterized by smaller cone angles, larger Q^2 values, and a higher plateau. The diffusion coefficient for each wobbling process is a function of both the cone angle, θ_c, and the correlation time, τ_c. For $\theta_c < 30°$, the relationship $\tau_c \simeq {\theta_c}^2/24D$ gives an accurate approximation to the more lengthy exact expression that should be used for larger angles.[57]

If the Si−OD reorients by more than one (independent) process, then the resultant correlation function can be expressed as the product of the individual correlation functions. For example, the anisotropy for an Si−OD that undergoes inertial motion and two separate wobbling-in-a-cone processes is given by

$$r(t) = 0.4T^2(S^2 + (1 - S^2)\exp[-t/\tau_{c1}])(R^2 + (1 - R^2) \times \exp[-t/\tau_{c2}]) \quad (6)$$

where T, S, and R are the order parameters for the inertial cone, first diffusive cone, and second diffusive cone, respectively. The correlation times, τ_{c1} and τ_{c2}, are for the first and second diffusive cones, respectively. The total order parameter, which determines the final plateau, is then given by ${Q_{total}}^2 = (TRS)^2$.

However, we should be careful before applying eq 6 to the data directly. As discussed above, the isotropic PP signal, $P(t)$, provided evidence of two surface sites with very different lifetimes, meaning that the total PSPP signal is the sum of the signals from the two components. Thus, the anisotropy should be analyzed from the perspective of a two-component system[59]

$$r(t) = \frac{a_{II}e^{-t/T_1^{II}}r(t)^{II} + (1 - a_{II})e^{-t/T_1^{I}}r(t)^{I}}{a_{II}e^{-t/T_1^{II}} + (1 - a_{II})e^{-t/T_1^{I}}} \quad (7)$$

where, for example, $r(t)^{II} = [S_{\parallel}^{II}(t) - S_{\perp}^{II}(t)]/[S_{\parallel}^{II}(t) - 2S_{\perp}^{II}(t)]$ is the anisotropy that would be observed if only component II were present. Equation 7 has been applied to various systems and, particularly, those in which water molecules are found in two distinct environments (with different lifetimes), such as the interfacial and core regions of reverse micelles[59] and Nafion fuel-cell membranes.[60] If the orientational dynamics for the two populations are the same, or $r(t)^{I} = r(t)^{II}$, then the total anisotropy will be equivalent to the individual component dynamics at all times. However, if $r(t)^{I}$ and $r(t)^{II}$ differ, then $r(t)$ becomes a more complex function of the individual component dynamics. As the time delay increases, the relative contribution of the shorter lifetime component to the total anisotropy will decrease. In systems with two-component dynamics, the anisotropy is often frequency dependent because the ratio of the two ensembles, which are reorienting in different manners, changes with frequency.

The solid curves in Figure 5a are fits of eq 7 to the CCl_4 anisotropy data (solid points). The fits describe the data quite well. The population fractions and vibrational lifetimes for the two silanol types, a_I, a_{II}, T_1^I, and T_1^{II}, were all known from fitting $P(t)$ as described in section III.B. These parameters were fixed in the fit of eq 7 to the data (since $a_I = 1 - a_{II}$, only one of these parameters is actually required). Additionally, the minimum number of cones needed to model $r(t)^{II}$ and $r(t)^{I}$, and obtain quantitative agreement with the data, was used. Ultimately, for the CCl_4 sample, $r(t)^{II}$ and $r(t)^{I}$ could be described with one inertial and one diffusive cone (eq 6, excluding the $R^2 + (1 - R^2)\exp[-t/\tau_{c2}]$ term) to obtain good agreement with the measured anisotropy.

A number of different fitting procedures were tested before arriving at the Figure 5a fit results. Fits that used the fewest parameters were given preference. The approach that we ultimately found successful was to only share the correlation times, τ_c. This approach suggests that the rate of diffusion depends on the vibrational frequency of the silanol, and this dependence can mainly be attributed to a change in the cone angle with frequency, which provides a measure of the steric restrictions of the local silanol environments.

In comparison to the CCl_4 sample, the Bz sample exhibits a much milder degree of frequency dependence, and attempts to fit the data to eq 7 with $r(t)^{II}$ and $r(t)^{I}$ unequal were not successful. The fit did not converge easily and gave unreasonably large cone angles for the type II silanols, suggesting that the rotational motion was essentially unrestricted. Inspection of the data in Figure 5b shows that the rotational dynamics become a little faster moving from the red side to the blue side of the band, but the overall shape of the decays does not change as dramatically as in the CCl_4 sample. The less-pronounced frequency dependence is also consistent with Figure 4d, which shows that the relative population fractions of type II and type I silanols do not change much over this frequency range. We found, instead, that using a one-component fit, in which $r(t)^{II}$ and $r(t)^{I}$ are equal, fits the Bz data much better (Figure 5b). One inertial cone and two diffusive cones were sufficient to model the data (eq 6). In this fit, the correlation times were shared across frequencies, while the cone angles were varied.

Table 2 displays the parameters obtained for type II and type I silanols near their absorption maxima at 2698 and 2720 cm^{-1}, respectively, in CCl_4 and at 2670 cm^{-1} (one-component fit) in Bz. These parameters were used in the chemical exchange modeling discussed below. The parameters for other frequencies are tabulated in the Supporting Information. In CCl_4, the type I silanols rotate at a faster rate than the type II silanols, since their cone angles are larger and τ_{c1} is smaller (1.0 vs 6.5 ps). This can be seen by considering Figures 5a and 4b together. As the

https://doi.org/10.1021/acs.jpcb.1c01225
J. Phys. Chem. B 2021, 125, 4566−4581

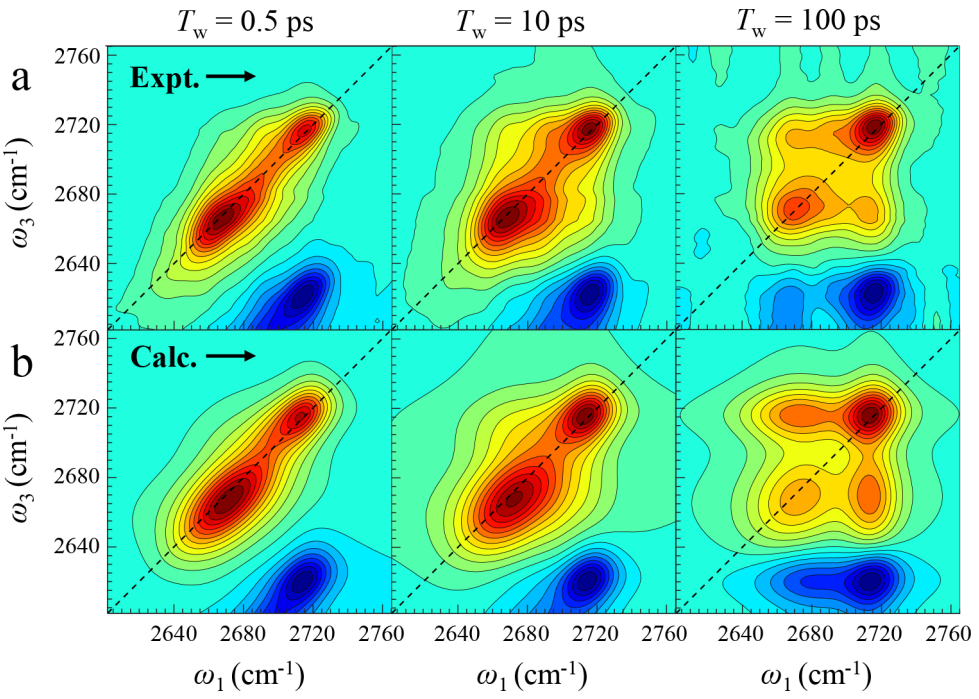

Figure 6. (a) Experimental 2D IR chemical exchange spectra in the isolated Si−OD stretching region for 1:5 benzene:CCl_4 in the pores of MCM-41 at T_w = 0.5, 10, and 100 ps. The red (positive) and blue (negative) peaks are from the 0−1 and 1−2 vibrational transitions, respectively. As T_w increases, off-diagonal peaks grow in as Si−OD/Bz complexes progressively form and dissociate. (b) Response function calculations of the data in (a) as described in section III.D.

frequency decreases, the type II silanol becomes a larger contribution to the observable, and the total anisotropy decays more slowly. These results suggest that type II silanols are in a slightly more restricted environment compared to the type I silanols. This might be the case if the type II silanols tend to be located near surface defects or cavities that have local environments that sterically hinder their wobbling motion. As discussed above, in Bz the dynamics of the type I and II silanols appear to converge. Overall, the dynamics in Bz become slower (τ_{c1} = 4.4 ps, τ_{c2} = 50 ps), and a larger range of angular space is sampled. This is evidenced by the appearance of a second diffusive cone in the orientational motion (not seen in CCl_4) potentially attributable to the Si−OD···π H-bond formed with Bz. This interaction may also be responsible for the smaller inertial cone angle in Bz compared to those in CCl_4 by reducing the range of motion on faster time scales. At the silica surface, the Bz molecule may shift and, perhaps, precess about the silanol. It may be energetically favorable for the Si−OD to be pulled around by the Bz molecule and still keep the π H-bond intact rather than sever the bond. Thus, the π H-bond may cause the silanol to sample a slightly larger angular space, albeit with a slower correlation time.

In summary, the rotational dynamics of the silanols were described with a wobbling-in-a-cone model. In CCl_4, the dynamics of the type I and II sites are more distinct, and the frequency dependence of the total anisotropy can be explained with a two-state model in which the two species each reorient in one inertial and one diffusive cone. Overall, the type II sites are located in more restricted environments (smaller cone angles) and sample the available angular space more slowly (longer correlation time) than type I sites. The weaker frequency dependence in Bz is indicative of more homogeneous dynamics, in which both sites reorient via one inertial and two diffusive cones. The more uniform and overall slower relaxation of silanols in Bz compared to CCl_4 was attributed to the Si−OD···π H-bond formed with Bz.

III.D. Chemical Exchange at Isolated Silanol Sites. 2D IR chemical exchange spectroscopy works in the following manner (see the Supporting Information for details).[21−23] The 2D IR experiment consists of three IR excitation pulses, which give rise to a fourth pulse, the vibrational echo. The heterodyne detected vibrational echo pulse is the signal. The first pulse in the sequence labels the vibrations of interest by their initial frequencies. The second pulse, arriving a short time later, stores the labeled information. After a waiting time, T_w, during which the system has time to evolve, the third pulse initiates a readout of the final frequencies, with the information carried by the vibrational echo pulse. 2D spectra are recorded as a function of T_w. As T_w increases, the system structure has more time to evolve, causing the 2D spectra to change. If there are two species, A and B, with resolvable frequencies in the FT-IR spectrum, at short time the two species will appear as bands in the 2D spectrum along the diagonal, a 45° line from the upper right to the lower left (high frequency to low frequency) of the spectrum. If A's convert into B's and B's turn into A's under equilibrium conditions (chemical exchange), then as T_w increases, off-diagonal peaks will appear in the spectrum, one from A's going to B's and one for B's going to A's. Because the system is in equilibrium, the growths of these two off-diagonal peaks are the same. Full analysis of the time-dependent growth of the off-diagonal peaks gives the time dependence of the interconversion of the two species.

A key observable that can further distinguish the isolated silanols is the dissociation time constant for the Si−OD···π H-bond complex formed with Bz obtained from 2D IR chemical exchange spectroscopy. Figure 6a displays 2D IR spectra of the isolated Si−OD stretching mode in 1:5 Bz:CCl_4 solution at waiting times, T_w, of 0.5, 10, and 100 ps. The red, positive peaks

https://doi.org/10.1021/acs.jpcb.1c01225
J. Phys. Chem. B 2021, 125, 4566−4581

are associated with the 0−1 vibrational transition, while the blue, negative peaks arise from the 1−2 transition. Similar to the PSPP signals, a small heating signal was observed in the 2D spectra and was removed as detailed in the Supporting Information. Because the molecular potential energy surface is anharmonic, the 1−2 transition is lower in energy than the 0−1 transition and is shifted below it along the ω_3 axis by the anharmonic shift, Δ.[35,37] At the earliest time of 0.5 ps, two bands are centered and elongated along the diagonal (the dotted line, $\omega_3 = \omega_1$). These 2D bands correspond to the 1D absorption bands shown in Figure 2 for the 1:5 Bz:CCl_4 solution (black curve). The lower frequency peak arises from silanols that are complexed with Bz, while the higher frequency peak arises from free silanols, those that are solvated by CCl_4. However, note that the preceding analyses indicate that each of these bands is composed of two underlying bands associated with two isolated silanol species: type I (isolated Q3) and type II (possible structure discussed below). Therefore, before any exchange has occurred, the complete 0−1 transition features are composed of a total of four peaks, two underlying each band.

For the longest waiting time, 100 ps, considerable exchange has occurred as shown by the off-diagonal peaks in the 2D spectrum. The upper-left cross-peak has its initial frequency, ω_1, at the lower frequency, indicating that the initial structure was an Si−OD complexed with Bz. Its final frequency, ω_3, is at the higher frequency, showing that the final structure is a free silanol. Therefore, the upper-left off-diagonal peak arises from free silanols that were initially involved in a chemical complex with Bz. In a similar manner, the lower-right cross-peak arises from complexed silanols that were initially free silanols. As these considerations suggest, population transfer from a diagonal peak to a cross-peak, or the reverse, can only occur along the ω_3 detection axis.[21] Molecules initially excited in a band with frequency (ω_1, ω_3) that undergo an exchange during the period T_w have a new ω_3 frequency when they are read out. They have the same ω_1 frequency because this is the frequency of the initial excitation. Therefore, after one exchange event, these molecules contribute to an off-diagonal band. If some silanols undergo two exchange events during T_w, they will have returned to their original diagonal peak. Therefore, molecules that make an odd number of exchanges contribute to off-diagonal bands, while molecules that undergo an even number of exchanges contribute to diagonal bands.[22] For completeness, we also consider the case in which silanols experience an *even* number of exchanges during T_w even though they do not contribute to the off-diagonal bands. Molecules that undergo an even number of exchanges affect the shape of the diagonal bands and, therefore, analysis of spectral diffusion.[22]

The T_w-dependent growth of the off-diagonal peaks directly tracks the formation and dissociation kinetics of the surface Si−OD···Bz complex.[21,22,45] Figure 6a displays the increasing relative amplitude of the cross-peaks with respect to the diagonal peaks as T_w increases. (Note that the data in each panel are normalized to the band with the greatest amplitude.) The time-dependent populations that give rise to the 2D diagonal and off-diagonal signals can be quantitatively described with a dynamic partition model that takes into account vibrational relaxation, chemical exchange, orientational relaxation, and the polarization configuration of the 2D IR experiment. Spectral diffusion of the transition will also influence the time-dependent 2D band shapes for silanols that have not undergone exchange.[22,45] However, spectral diffusion does not affect the populations of the associated species (or volumes of their peaks) and therefore does not enter into the dynamic partition model because the peak volumes are used.[22,45] Vibrational relaxation will cause all peaks to decrease in amplitude, regardless of polarization, as the Si−OD stretch relaxes from the first excited vibrational state to the ground state. Chemical exchange will cause the off-diagonal peaks to grow in and the diagonal peaks to decay, although the presence of even exchanges will lead to a small degree of refilling of the diagonal populations. The effect of orientational relaxation of the silanols on the 2D signal depends on the polarization configuration. In the "perpendicular" configuration, $\langle XXYY\rangle$, the first two pump interactions are $\hat{Y}$ polarized, while the probe and detection polarization are $\hat{X}$ polarized. The contribution of a dipole to the signal is determined by the projection of the dipole onto the polarization of the fields at the time of each interaction, and the final signal magnitude is determined by its projection onto the detection direction.[35,36,50] In $\langle XXYY\rangle$, molecules are preferentially excited in the $\hat{Y}$ direction, but reorientation during T_w causes them to contribute *more* to the detected signal in the orthogonal direction, X, leading to a signal growth. Here, all experiments were performed in $\langle XXYY\rangle$ to obtain reliable, scatter-free data.[31,33,61] Therefore, all of the peaks in the 2D spectrum will experience a growth originating from the wobbling motion of the silanols, and the off-diagonal peaks will have additional growth caused by exchange.

The quantitative details of the dynamic partition model are described further in the Supporting Information and elsewhere.[22,62] It is illustrated schematically in Figure 7. As discussed

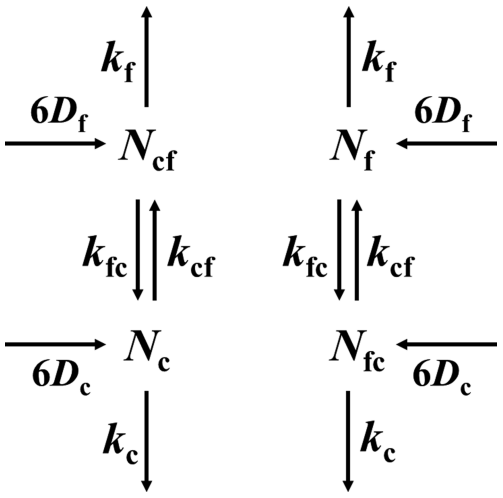

Figure 7. Kinetic scheme illustrating the various sources (inward arrows) and sinks (outward arrows) controlling the effective diagonal and off-diagonal peak populations for $\langle XXYY\rangle$ and a single silanol type. Parameter definitions are provided in section III.D. Any time dependence has been suppressed for clarity.

in the Supporting Information, the solution for $\langle XXYY\rangle$ and a single chemical exchange system is given by

$$\begin{pmatrix} N_f(t) \\ N_{cf}(t) \\ N_c(t) \\ N_{fc}(t) \end{pmatrix} = \frac{15}{9}\left(\exp[\mathbf{A}t] - \frac{2}{5}\exp[\mathbf{B}t]\right)\begin{pmatrix} N_f(0) \\ N_{cf}(0) \\ N_c(0) \\ N_{fc}(0) \end{pmatrix} \quad (8)$$

where the effective populations $N_f(t)$, $N_c(t)$, $N_{cf}(t)$, and $N_{fc}(t)$ are respectively the total diagonal free population, the total

https://doi.org/10.1021/acs.jpcb.1c01225
J. Phys. Chem. B 2021, 125, 4566−4581

diagonal complex population, the off-diagonal population that was complexed and became free (odd exchanges), and the off-diagonal population that was free and become complexed (odd exchanges). In eq 8, the anisotropic matrix, **B**, is given by

$$\mathbf{B} = \begin{pmatrix} -[k_f + k_{fc} + 6D_f(t)] & 0 & 0 & k_{cf} \\ 0 & -[k_f + k_{fc} + 6D_f(t)] & k_{cf} & 0 \\ 0 & k_{fc} & -[k_c + k_{cf} + 6D_c(t)] & 0 \\ k_{fc} & 0 & 0 & -[k_c + k_{cf} + 6D_c(t)] \end{pmatrix} \tag{9}$$

where $k_f = 1/T_{1,f}$ and $k_c = 1/T_{1,c}$ are the inverse lifetimes of the free and complex species, respectively, k_{fc} is the rate of complexation, k_{cf} is the rate of dissociation, and $6D_f(t)$ and $6D_c(t)$ are the rates of rotation for the free and complex species, respectively. The isotropic matrix, **A**, is independent of rotation and is the same as **B** excluding the $6D_f(t)$ and $6D_c(t)$ terms. Here, we have taken the approach of Ji et al. (see the Supporting Information) and used effective time-dependent diffusion coefficients, $D_\alpha(t)$, to include restricted orientational diffusion in the kinetic model,[63] where $C_{2,\alpha}(t)$ is the wobbling-in-a-cone orientational correlation function for the α state. The discussion in the Supporting Information also describes how oscillators that exchange an even number of times can be distinguished from those that do not exchange.

To describe a system in dynamic equilibrium, one must specify the dissociation time constant, $\tau_d = k_{cf}^{-1}$, and the equilibrium constant, K_{eq}, for the exchange reaction F ⇌ C. The association time constant, $\tau_a = k_{fc}^{-1}$, can be determined from τ_d and K_{eq} by using the equilibrium condition, $K_{eq} = k_{fc}/k_{cf} = \tau_d/\tau_a$. Two approaches have been used to extract τ_d from chemical exchange spectra.

In the first approach, the experimental 2D spectra are fit with a combination of 2D Gaussians.[22] The volumes of the Gaussian fits provide the time-dependent peak volumes. To arrive at effective populations for the different species, the peak volumes are rescaled by dividing out the transition dipole moments of the contributing species.[22] The populations are then fit to the dynamic partition model for the chemical exchange process to obtain the parameter τ_d. The second approach uses the third-order material response functions from time-dependent diagrammatic perturbation theory to fit the 2D band shapes.[22] The dynamic partition model is incorporated into the response functions, $R(t_3,T_w,t_1)$, so that the amplitudes of the various peaks are consistent with a chemical exchange system. Specifically, the solution to the dynamic partition model provides the time-dependent populations for the various peaks. The population associated with a particular response function is included as an additional multiplicative factor in the response function.[22]

A key difference between these two approaches is that in the first method the peak volumes are determined first and the dynamic partition model is applied second, while in the second method, the volume fitting and application of the model are done simultaneously. This difference ultimately led us to select the second approach for the silica system. The antidiagonal width and spectral overlap of the peaks made extracting the cross-peak volumes with 2D Gaussian fits challenging at early time, leading to nonzero cross-peak volumes when extrapolated to time zero. In the response function approach, the inclusion of the dynamic partition model in the peak fitting imposes the constraint that the cross-peaks must extrapolate to zero volume at zero time. Additionally, this approach allows us to better model the time-dependent band shapes with the frequency–frequency correlation function (FFCF),[22] which can generate various band shapes ranging from homogeneous (Lorentzian) to inhomogeneous (Gaussian) line shapes (see the Supporting Information).[35] Lastly, we find that this approach is preferable when the system is composed of more than one exchanging ensemble. In this situation, two isolated silanol types are undergoing chemical exchange. Twice the usual number of peaks (12 in total for the 0–1 transition) is needed to model the spectra. Applying the peak fitting and dynamic partition model at the same time makes the determination more reliable for the reasons discussed above.

The experimental 2D spectra in Figure 6a were fit with the response function expressions delineated by Kwak et al. and described in the Supporting Information.[22] All of the data suggests that the signal arises from two different isolated silanol species. Thus, we treated the total system as the sum of two independently exchanging subsystems for the type I and II silanols. Isolated silanols are too distant from each other to hydrogen-bond; therefore, it is reasonable to assume that their exchange dynamics are not influenced by neighboring silanols. In this model, the system can be viewed as a weighted sum of two equilibria, one for each silanol type

$$[1 - a_I]\{F^{II} \underset{k_{cf}^{II}}{\overset{k_{fc}^{II}}{\rightleftharpoons}} C^{II}\} + a_I\{F^{I} \underset{k_{cf}^{I}}{\overset{k_{fc}^{I}}{\rightleftharpoons}} C^{I}\} \tag{10}$$

where $a_I = 1 - a_{II}$ is the relative population fraction of the type I site, first defined in section III.B. Here, the parameter is understood to be integrated over the entire band and independent of the solvent.

Given the complexity of this system, any reasonable assumptions that reduce the number of parameters in the model were taken. For example, in separating the isotropic PP spectra into type I and II bands in Figure 4, we made the assumption (also made by others[64]) that the transition dipole moment was the same for both silanols (I and II) in a single solvent. This implies that the ratio $|\mu_c|^2/|\mu_f|^2$ is also identical for I and II. The $|\mu_{12}|^2/|\mu_{01}|^2$ ratios for the free and complex forms were similarly taken to be the same for both silanols. Additionally, we assumed that K_{eq} is the same for I and II. This was motivated by the observation that the linear absorption spectrum for the mixed solvent can be fit with a linear combination of the pure solvent spectra (see Figure 2). If this were not possible, it would suggest that the two bands from I and II were not changing in equal proportion in the mixed solvent system, and the K_{eq}'s for the two sites are different. We also assumed that spectral diffusion, and thus the FFCF, only depends on whether a silanol is in the free or complex form (and is independent of silanol type). As noted previously, the exchange rate and FFCF are relatively independent.[22] The exchange rate dictates the growth of the off-diagonal peaks, causes the diagonal peaks to decay, and also influences the shape

https://doi.org/10.1021/acs.jpcb.1c01225
J. Phys. Chem. B 2021, 125, 4566–4581

Table 3. Chemical Exchange Fit Parameters

silanol	a_I	K_{eq}	$\lvert\mu_c\rvert^2/\lvert\mu_f\rvert^2$	τ_d (ps)	Δ_f (cm^{-1})	Δ_c (cm^{-1})
II		0.8 ± 0.1	2.0 ± 0.3	4.0 ± 0.8	101 ± 4	94 ± 1
I	0.7 ± 0.1	0.8 ± 0.1	2.0 ± 0.3	82 ± 15	95 ± 1	92 ± 2

of the diagonal peaks. The FFCF only influences the time-dependent shape of the diagonal peaks but has no influence on the growth of the off-diagonal peaks.

Therefore, the adjustable parameters in the fit were $\lvert\mu_c\rvert^2/\lvert\mu_f\rvert^2$, K_{eq}, the dissociation rates, k_{cf}^{I} and k_{cf}^{II}, and the FFCF for the complex and free transitions. The vibrational lifetimes and orientational relaxation parameters determined for the type II and I transitions located at ~2698 and ~2720 cm^{-1} in CCl_4 and at 2670 cm^{-1} in Bz were used as input parameters (Table 2). The peak centers were permitted to adjust within a few cm^{-1} of these positions given some uncertainty in the precise location of the bands and the limited resolution of the 2D IR spectrometer (~1.3 cm^{-1}) in this frequency range. The orientational relaxation parameters were not adjusted as is sometimes done to account for the change in viscosity going from the pure solvents to the mixed solvent. We have no way of determining the viscosity of the mixed solvent confined in the 2.8 nm MCM41 pores, and it is likely a local property that depends on position in the pore. The FFCFs for the diagonal complex and free peaks were initialized with the FFCFs extracted from the pure Bz and CCl_4 2D IR spectra (see the Supporting Information), which each contain a homogeneous term, three exponentials, and a static inhomogeneous term.

The 2D spectra at all T_w values were simultaneously fit to the two-component chemical exchange model discussed above. A nonlinear least-squares solver in MATLAB R2019a using the "trust-region-reflective" algorithm was used to iterate the parameters and minimize the residuals. Three independent experiments were fit, and the resulting parameters were averaged together. The results are shown in Figure 6b below the corresponding measured spectra in Figure 6a. Overall, the essential features of the spectra are reproduced, and the agreement is quite good. At 100 ps, the fit does slightly underestimate the intensity of the lower frequency diagonal peak corresponding to the Si−OD/Bz complex, and it slightly overestimates the magnitude of the cross-peaks. Note, however, that the spectra are not plotted on the same scale for better visualization of their features. In reality, the signal has substantially decayed by 100 ps. Poorer agreement between the experiment and model is unavoidable at longer T_w because of the reduced signal-to-noise and lower absolute signal amplitude that result from vibrational relaxation.

Table 3 displays key parameters from the fit. The modeling indicates that type I silanols make up 70 ± 10% of the total isolated silanol population probed in these experiments; thus, the type II species makes up 30 ± 10%. This ratio is very close to the 4:1 ratio of nonacidic to acidic silanol sites measured experimentally with SHG.[18] The 4:1 ratio appears to be ubiquitous in studies of the amorphous silica surface, and its molecular origins are still unclear.[16] It has been assigned, for example, to the ratio of H-bonded to isolated silanols[16] as well as the ratio of geminal Q2:isolated Q3 sites.[65] *Ab initio* MD simulations suggest that assigning the two acidity groups to two specific silanol types is not possible.[16,17,19] In this study, we have assigned the type I silanol to the isolated Q3 structure. We refrain from assigning a definitive structure to the type II silanol. The type II site is a significant fraction of the population, but the results suggest that it is a minor species relative to type I.

The dissociation time constants, τ_d, for the type II and I silanols are dramatically different at 4.0 ± 0.8 and 82 ± 15 ps, respectively. This difference is illustrated in Figure 8. The total

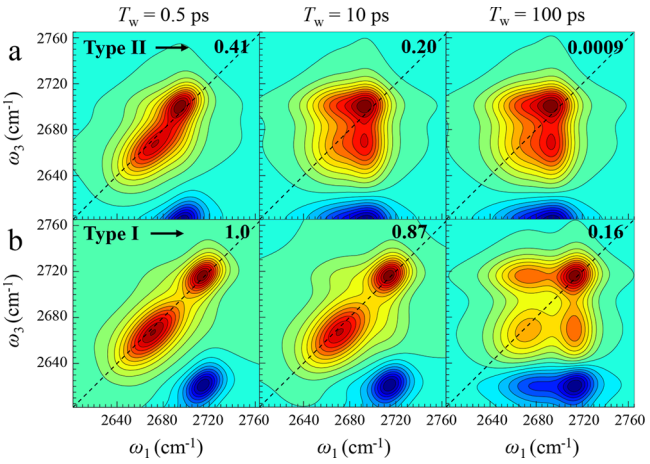

Figure 8. Calculated chemical exchange spectra from Figure 6b separated into contributions from (a) type II and (b) type I isolated silanols. The rapid exchange occurring at the type II site can be observed by the comparatively faster growth of its off-diagonal chemical exchange peaks. The spectra are plotted on different scales to clearly observe the contours at longer time delays. To provide a sense of their relative magnitudes, the maximum value of each spectrum is ratioed to that of the type I spectrum at 0.5 ps and shown in the upper right.

calculated 2D spectra (Figure 6b) were decomposed into the contributions from type II (Figure 8a) and type I (Figure 8b) silanols. The spectra are plotted on different scales for better visualization of the contours at longer time delays. The development of cross-peaks is very rapid for the type II silanols and looks essentially complete by 10 ps, whereas the cross-peak growth is just getting underway for the type I silanols. Also, observe that the total 2D spectrum at 100 ps (Figure 6b) is essentially equivalent to the type I 2D spectrum (Figure 8b) at that time. This is because of the very short vibrational lifetime of the type II site in either solvent, which causes the signals from all type II peaks to completely decay by 100 ps. The maximum value of each spectrum, normalized to that of the type I, 0.5 ps spectrum, is shown in the upper right of each spectrum to provide a better sense of how the population fractions and lifetimes influence the contributions of the two components at each T_w. At long times, the signal from the type I site is the only significant contribution. The result, $\lvert\mu_c\rvert^2/\lvert\mu_f\rvert^2$ = 2.0 ± 0.3 (Table 3), obtained here is slightly larger but still within error of the value (1.7) obtained for deuterated triethylsilanol in a 4:5 Bz:CCl_4 bulk solvent mixture.[45] Also, in that study, an equilibrium constant K_{eq} = 1 was obtained versus K_{eq} = 0.8 ± 0.1 obtained here for 1:5 Bz:CCl_4 (Table 3). Despite an almost 3-fold reduction in the Bz mole fraction, K_{eq} is barely changed. This difference reflects the greater preference of the silica surface silanols for Bz relative to triethylsilanol.

https://doi.org/10.1021/acs.jpcb.1c01225
J. Phys. Chem. B 2021, 125, 4566−4581

The time-dependent populations of the 0−1 diagonal free peak (black squares), diagonal complex peak (red circles), and off-diagonal peaks (green down and blue up triangles) are plotted in Figure 9 for the (a) total, (b) type II, and (c) type I

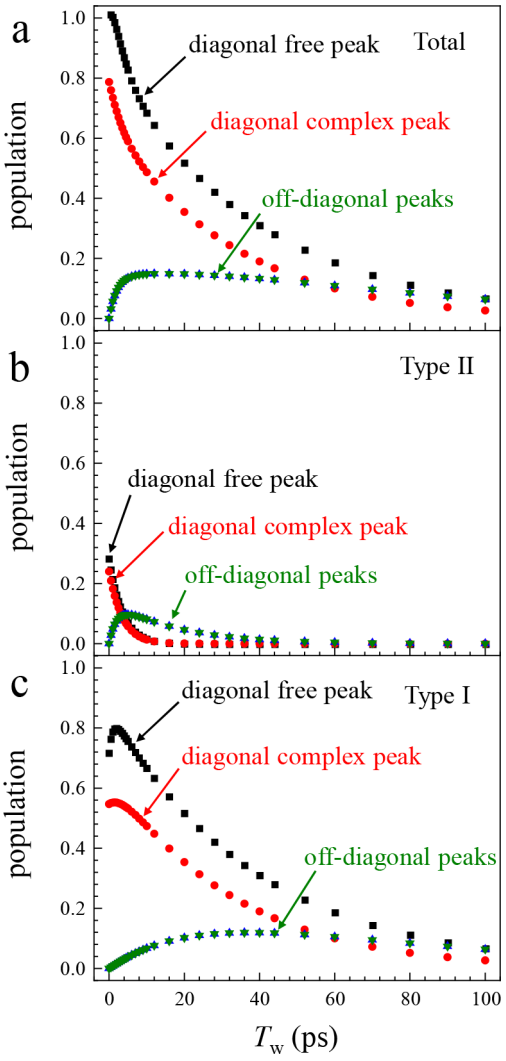

Figure 9. Calculated time-dependent effective populations associated with the diagonal free (black squares), diagonal complex (red circles), and off-diagonal (green down and blue up triangles) peaks for the (a) total, (b) type II, and (c) type I isolated silanol chemical exchange systems. The growth of the diagonal effective populations from the wobbling-in-a-cone reorientational motion is most evident for the type I silanols because of their longer vibrational lifetime.

systems. The populations were obtained by rescaling the peak volumes by $|\mu_\alpha|^4$ for the diagonal peaks and $|\mu_\alpha|^2|\mu_\beta|^2$ for the off-diagonal peaks.[22,45] The volumes were obtained by separately Fourier transforming the response functions associated with each peak and integrating the peak. (Recall that the diagonal peaks for a given silanol type have two contributions, i.e., either zero or an even number of exchanges). All of the populations in Figure 9 have been normalized to (divided by) the total diagonal free peak population at time zero, $N_f(0)$. Figure 9 contains important features, which are difficult to discern from 2D contour plots. The rapid growth and decay of the type II off-diagonal peaks are clearly illustrated in Figure 9b. The rapid growth and decay are caused by the fast 4.0 ps dissociation time and short vibrational lifetimes of the free (17.8 ps) and complex (15 ps) forms In contrast, the type I off-diagonal peaks in Figure 9c grow in at a much slower pace (τ_d = 82 ps) and linger for much longer because of the longer vibrational lifetimes of the free (71 ps) and complex (46.7 ps) forms. Another noteworthy consequence of the longer vibrational lifetimes is that the growth of the diagonal free and diagonal complex effective populations caused by wobbling-in-a-cone reorientation is clearly observed for type I silanols (Figure 9c) as the rises in the populations at very short times. In the case of type II sites, the short lifetimes cause a rapid decay of the diagonal peaks that obscures the growth from reorientation. In total, the influence of rotation is faintly observed and is only discernible at the shortest times for the diagonal free peak (Figure 9a).

The FFCFs corresponding to the complex and free forms of both type I and II peaks are tabulated in Table 4. Given the complexity of this system, and our assumption that spectral diffusion is only dependent on whether a silanol is in the free or complex form, the FFCF parameters should be considered estimates. We did test the more general case of including one set of FFCFs per silanol type (a total of 4); however, this greatly increased the number of parameters in the fit without significantly changing the resulting dissociation time constants. As mentioned above, this is expected, as the FFCF has no influence on the growth of the off-diagonal peaks. Perhaps the most interesting aspect of the FFCFs is that they contain a static inhomogeneous term, Δ_4. This means that the diagonal peaks (no exchange) will maintain some degree of correlation, or nonzero CLS,[24,61] on long time scales compared to the experimental time window. Although the silanols appear to have similar characteristics within a given type, including vibrational lifetime, reorientation, and dissociation time constants, this static inhomogeneity indicates that they still individually experience unique structural environments on the amorphous silica surface that do not interconvert on the time scale of the experiments. Therefore, it is not possible for silanols to sample all possible structural environments that contribute to the inhomogeneous line. If the surface structure were more dynamic, or processes like surface migration were significant, the static inhomogeneity would be reduced or nonexistent.

In summary, the Si−OD/Bz complex dissociation times for type II and I silanols were determined to be 4.0 ± 0.8 and 82 ± 15 ps, respectively, by modeling the growth of off-diagonal chemical exchange peaks in the 2D IR spectra of the mixed solvent system. The two silanol types were treated as independent chemical exchange subsystems, with the total spectrum given by the sum of the type I and type II spectra. The lifetime and orientational relaxation parameters from the PSPP

Table 4. FFCF Parameters from Chemical Exchange Fit[a]

	T_2^* (ps)	Δ_1 (cm^{-1})	τ_1 (ps)	Δ_2 (cm^{-1})	τ_2 (ps)	Δ_3 (cm^{-1})	τ_3 (ps)	Δ_4 (cm^{-1})
free	1.2 ± 0.3	9 ± 1	0.5 ± 0.1	2.5 ± 0.1	5.6 ± 0.2	2.2 ± 0.2	55.4 ± 0.1	5.2 ± 0.1
complex	0.5 ± 0.1	5 ± 1	0.14 ± 0.1	6 ± 1	6.8 ± 0.3	8 ± 1	38.1 ± 0.5	12.7 ± 0.6

[a]The parameters are described in the Supporting Information.

https://doi.org/10.1021/acs.jpcb.1c01225
J. Phys. Chem. B 2021, 125, 4566−4581

measurements were fixed parameters in the dynamic partition model, and the spectral diffusion parameters for the diagonal peaks were initialized with the parameters from the pure solvent systems.

III.E. Significance of Complex Dissociation Times. In this section, we focus on the dissociation time constant because it is independent of the benzene concentration. The large difference in dissociation times obtained for type I and II silanols is particularly striking. To our knowledge, there are no studies that have measured exchange times at solid/liquid interfaces on these time scales. Previously, τ_d for deuterated triethylsilanol in bulk 4:5 Bz:CCl_4 was measured to be 9 ± 2 ps.[45] The type II silanols exchange slightly faster at 4.0 ps, and the type I silanols exchange substantially slower at 82 ps. Thus, depending on the nature of the silanol, the exchange rate can be similar to or much slower than the analogous bulk liquid chemical exchange reaction.

We can make use of a valuable finding by Zheng and Fayer[45] to relate the dissociation times to the enthalpy of the formation of the complexes. Zheng and Fayer measured the dissociation time constants for 13 complexes involving the formation of H-bonds, mainly π H-bonds, with a hydroxyl. Eight of these were complexes of phenol with benzene and substituted benzenes, such as toluene. The other five were complexes with triethylsilanol. Of these, four were with benzene and substituted benzenes and one was with acetonitrile. When the dissociation times, τ_d, were plotted against $\exp[-\Delta H^0/RT]$ where ΔH^0 is the enthalpy of formation of the complexes, the 13 data points fell on a line. Therefore, the dissociation times are correlated to the enthalpy of formation. Figure 10 is a plot of the previous data, in which both τ_d and ΔH^0 were measured.[45] The black points are the phenol complexes, and the blue points are the triethylsilanol complexes. The red points are the surface silanol/benzene complex dissociation times measured here placed on the line at the appropriate positions.

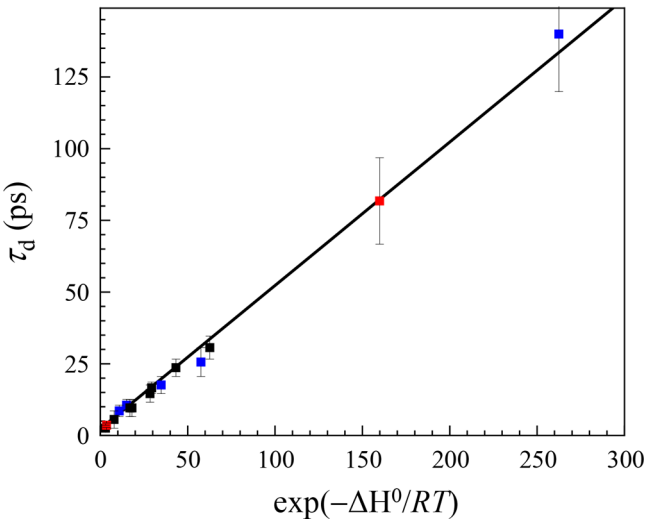

Figure 10. Plot of data previously reported in the literature (black points and blue points), in which both τ_d and ΔH^0 were measured and the linear fit (black line) to the data.[45] The black points are complexes of benzene and benzene derivatives with the hydroxyl of phenol, and the blue points are complexes of benzene, benzene derivatives, and acetonitrile with the hydroxyl of triethylsilanol. The red points are the surface silanol/benzene complex dissociation times, τ_d, measured here and placed on the line at the appropriate positions, yielding their values of ΔH^0.

A fit to the prior data gives the following relationship[45]

$$\tau_d = B + A^{-1} \exp[-\Delta H^\circ/RT] \quad (11)$$

where B = 2.3 ps and A^{-1} = 0.5 ps. Given that this relationship holds for phenol with benzene and benzene derivatives, triethylsilanol with benzene and benzene derivatives, and even triethylsilanol with acetonitrile, it is reasonable to assume that this relationship holds for the complexes between Bz and type I and II silanols, which also involve an H-bond with a silanol hydroxyl. Using eq 11 gives $\Delta H^0 = -0.6$ kcal/mol for II and $\Delta H^0 = -3.0$ kcal/mol for I at 295 K.

We can compare the ΔH^0 values determined here to an older study by Morimoto and Naono, who used adsorption calorimetry to measure the heat of adsorption (ΔH^0) of Bz on silica gel from a cyclohexane solution at 30 °C.[66] They found that ΔH^0 increased in magnitude for silica gels activated at increased temperatures. The values were −1.2, −1.6, −2.0, and −3.8 kcal/mol on samples treated at 100, 300, 500, and 800 °C, respectively. At the same time, they found the silanol content and total amount of Bz adsorbed on the silica gel both decreased with increasing activation temperature. Remarkably, the ratio of adsorbed Bz per silanol group increased as a function of increasing activation temperature. On the basis of these findings, they concluded that silanol groups on the surfaces treated at higher temperatures attracted Bz more strongly than those on the surfaces treated at lower temperature.

From the data of Morimoto and Naono, it can be seen that the ΔH^0 values obtained from our measured τ_d, by using the relationship of Zheng and Fayer, are reasonable. However, the ΔH^0 from the calorimetry experiments is an average over the entire silanol population on the silica gel surface. For comparison, it is better to take a weighted average of the estimated ΔH^0 for the type I (70%) and II (30%) silanols obtained here. The result is $\Delta H^0_{avg} = -2.3$ kcal/mol, which falls nicely within the range of values they measured. However, this comparison is approximate, as our measurement does not include the effect of H-bonding silanols, which also enter into the calorimetry measurements. Nonetheless, the increased exothermicity with increased activation temperature can be qualitatively rationalized based upon our measurements. The type II silanols, which are associated with the smaller ΔH^0 value, have been shown to be preferentially removed with increasing activation temperature.[14] Thus, with increasing temperature, the type I isolated Q3 silanols comprise a larger portion of the average, leading to an increasingly exothermic (more negative) ΔH^0_{avg}.

What determines the large difference in dissociation times of Bz on the two sites? Rimola et al. studied the adsorption of Bz on dehydroxylated and hydroxylated silica surface models at the *ab initio* level with DFT methods.[39] Plain DFT methods using common GGA functionals, including hybrids like B3LYP, significantly underestimate the adsorption energies (from the gas phase) obtained from experimental adsorption isotherms by ∼30−40 kJ/mol. While they can reasonably describe H-bonding interactions, they do not account for van der Waals (dispersive) forces.[39,67] When an energy correction is applied to account for dispersive forces, the calculated energies are in much better agreement with experiments, indicating the importance of both H-bonding and dispersive forces.[39] Nonspecific van der Waals interactions between the adsorbate and surface can influence the complex geometry by distorting the directional H-bonding

https://doi.org/10.1021/acs.jpcb.1c01225
J. Phys. Chem. B 2021, 125, 4566−4581

interactions.[67] In light of these findings, the substantially longer dissociation time for isolated Q3 silanols may be attributed not only to the ability of the delocalized electron cloud of the Bz ring to form a relatively stronger π H-bond with the OD but also to the ability of the molecule to maximize van der Waals interactions with the surrounding surface. It seems that the best way to optimize both contributions is for the Bz molecule to lie relatively centered on the silanol, close in and with its ring parallel to the surface.[39] On the other hand, the type II site may be associated with surface defects which sterically force Bz to adopt a configuration that disrupts both interactions or compromises one type of interaction in favor of the other. If the type II silanol is indeed a vicinal silanol, as has been suggested,[14,64] it may be the case that in attempting to center the ring on one silanol the relatively positive CH regions become involved in destabilizing repulsive interactions with hydrogen of the neighboring silanol.

Crystal violet (CV^+) adsorption onto the deprotonated silanols of planar silica in acetonitrile has been studied with reflection SHG[25] and evanescent-wave cavity ring-down spectroscopy.[26] These studies found evidence of CV^+ adsorption onto two silanol types as well, which they similarly denote type I and II. The authors found that the free energy of adsorption of CV^+ onto the type I and II sites was respectively ~−30 kJ/mol and somewhere in the range of −12 to −18 kJ/mol. They propose that the type I silanol is surrounded by a large empty surface area, which accommodates the large size (~120 Å^2) of CV^+, suggesting it is also of the isolated Q3 type.[25,26] The more favorable adsorption of CV^+ onto the type I site is consistent with the present findings for Bz. They propose that the type II site has a nearby OH group that interacts repulsively with the positively charged CV^+, suggesting that it could be a vicinal site or a site within a relatively dense silanol region. A difference between the CV^+ studies and the present work is that the relative populations of the two sites are reversed in the CV^+ studies, with the type I site being ~30% of the total population. The difference may arise from the fact that H-bonding silanols also contribute in those studies and will most likely fall in their type II category. Here, we have limited our signal to the isolated Si−OD stretching region of the IR spectrum. Therefore, only vicinal or geminal isolated silanols can present two hydroxyl groups in close proximity. Although we cannot completely rule out geminal silanols as the identity of the type II site, geminal silanols do not condense as favorably as vicinal silanols,[9,10] which would seem to contradict the dramatic temperature dependence of the lower frequency type II band.[14] Moreover, geminal silanols are thought to be spectroscopically indistinguishable from isolated Q3 silanols.[10,68,69] Further investigations are needed to elucidate the detailed structure of the type II silanols.

IV. CONCLUDING REMARKS

The reversible adsorption of Bz on the amorphous silica surface has been probed with 2D IR chemical exchange spectroscopy as well as polarization selective pump−probe experiments and FT-IR spectroscopy. For H-bond acceptor molecules such as Bz, silanol groups serve as active sites for the adsorption process. Thus, we studied the isolated Si−OD stretching vibrational mode, which is a local probe of the intrinsic surface dynamics and is directly involved in the chemical exchange process. The vibrational lifetime and orientational relaxation of the isolated silanols were measured with PSPP experiments, and the adsorption/desorption of Bz on the surface, from a benzene/carbon tetrachloride solution, was directly observed with 2D IR chemical exchange spectroscopy.

One short and one long vibrational lifetime were measured and found to be associated with two IR-active modes that heavily overlap in the linear and third-order spectra. The long lifetime is associated with the main absorption feature and was assigned to the Si−OD stretching mode of isolated Q3 silanols, which, in keeping with convention, was designated type I.[14,25,26] The remaining mode with the shorter lifetime was designated type II. While the type I lifetime decreased significantly upon the formation of a π H-bond with Bz, the type II lifetime was effectively insensitive to whether the silanol was in the presence of CCl_4 or Bz. These results suggest that type II sites have a greater tendency to interact with the silica surface than the adjacent solvent.

Orientational relaxation measurements revealed that isolated silanols are surprisingly free to undergo orientational motions relative to other surface bound hydroxyl groups.[24] The rotational motion of the individual silanol populations was interpreted within the framework of the wobbling-in-a-cone model of restricted angular diffusion.[56−58] In the weakly interacting solvent CCl_4, the dynamics of the two sites are more distinct, and the frequency dependence of the orientational correlation function can be explained with a two-state model. The weaker frequency dependence in Bz is indicative of more homogeneous dynamics. The π H-bond interaction appears to cause the silanols to rotate to some extent as a single moiety and significantly slows the angular sampling.

The 2D IR measurements revealed the growth of off-diagonal chemical exchange peaks for silanols in the mixed solvent, showing that the free (Si−OD···CCl_4) and complex (Si−OD···Bz) silanols are in dynamic equilibrium at the surface. The dissociation times for the Si−OD···π H-bonds formed between Bz and the type I and II silanols were determined by fitting the spectra with a two-site dynamic partition model and response function calculations to describe the time-dependent populations and their 2D band shapes. The data analysis revealed rapid and slow dissociation time constants of 4.0 and 82 ps for type II and I silanols, respectively. The former is slightly faster than the dissociation time for triethylsilanol in bulk solution, while the latter is nearly an order of magnitude slower.

Using the dissociation times, we determined the enthalpies of formation of the surface complexes to be −0.6 and −3.0 kcal/mol for type II and I, respectively. Stronger van der Waals interactions between Bz and the surface surrounding the type I site likely play a role in determining its longer dissociation time and more exothermic ΔH^0. The type I site may be located in regions that are relatively flatter and defect free compared to the type II site, allowing Bz to approach the silanol more closely and optimize its contact with the surface. This could lead to a cooperative effect between H-bonding and dispersive forces for the type I complex. In contrast, the similarity between the type II dissociation time and that of triethylsilanol in bulk solution suggests that dispersive forces contribute more weakly to the interaction.

This work used 2D IR chemical exchange spectroscopy, which is a powerful method that can be used for elucidating complex heterogeneous dynamics occurring at surfaces and interfaces. The results yield the dynamics of the formation and dissociation of surface complexes at distinct surface sites of nanoporous silica as well as structural information and the energetics of complex formation.

https://doi.org/10.1021/acs.jpcb.1c01225
J. Phys. Chem. B 2021, 125, 4566−4581

■ ASSOCIATED CONTENT

Supporting Information

The Supporting Information is available free of charge at https://pubs.acs.org/doi/10.1021/acs.jpcb.1c01225.

Optical methods, heating signal subtraction methods, chemical exchange theory, pure solvent 2D IR spectra and CLS, tables of $P(t)$, $r(t)$, CLS, and FFCF parameters for the pure solvent systems (PDF)

■ AUTHOR INFORMATION

Corresponding Author

Michael D. Fayer − *Department of Chemistry, Stanford University, Stanford, California 94305, United States;* orcid.org/0000-0002-0021-1815; Phone: (650) 723-4446; Email: fayer@stanford.edu

Authors

Steven A. Yamada − *Department of Chemistry, Stanford University, Stanford, California 94305, United States;* orcid.org/0000-0003-3171-1625

Samantha T. Hung − *Department of Chemistry, Stanford University, Stanford, California 94305, United States;* orcid.org/0000-0001-9448-0962

Jae Yoon Shin − *Department of Advanced Materials Chemistry, Korea University, Sejong, Korea;* orcid.org/0000-0002-8884-9687

Complete contact information is available at: https://pubs.acs.org/10.1021/acs.jpcb.1c01225

Notes

The authors declare no competing financial interest.

Data are available by contacting Professor Michael D. Fayer, Department of Chemistry, Stanford University, Stanford, CA 94305-5080. Email: fayer@stanford.edu.

■ ACKNOWLEDGMENTS

This work was funded by the Division of Chemical Sciences, Geosciences, and Biosciences, Office of Basic Energy Sciences of the U.S. Department of Energy through Grant DE-FG03-84ER13251 (S.A.Y. and M.D.F.). S.A.Y. gratefully acknowledges the support from a Stanford Graduate Fellowship.

■ REFERENCES

(1) Parida, S. K.; Dash, S.; Patel, S.; Mishra, B. K. Adsorption of organic molecules on silica surface. *Adv. Colloid Interface Sci.* **2006**, *121* (1), 77−110.

(2) Cashin, V. B.; Eldridge, D. S.; Yu, A.; Zhao, D. Surface functionalization and manipulation of mesoporous silica adsorbents for improved removal of pollutants: a review. *Environ. Sci. Water Res. Technol.* **2018**, *4* (2), 110−128.

(3) Fang, Y.; Lakey, P. S. J.; Riahi, S.; McDonald, A. T.; Shrestha, M.; Tobias, D. J.; Shiraiwa, M.; Grassian, V. H. A molecular picture of surface interactions of organic compounds on prevalent indoor surfaces: limonene adsorption on SiO_2. *Chem. Sci.* **2019**, *10* (10), 2906−2914.

(4) Rimola, A.; Costa, D.; Sodupe, M.; Lambert, J.-F.; Ugliengo, P. Silica Surface Features and Their Role in the Adsorption of Biomolecules: Computational Modeling and Experiments. *Chem. Rev.* **2013**, *113* (6), 4216−4313.

(5) Bolis, V.; Fubini, B.; Marchese, L.; Martra, G.; Costa, D. Hydrophilic and Hydrophobic Sites on Dehydrated Crystalline and Amorphous Silicas. *J. Chem. Soc., Faraday Trans.* **1991**, *87* (3), 497−505.

(6) Gierada, M.; Petit, I.; Handzlik, J.; Tielens, F. Hydration in Silica Based Mesoporous Materials: A DFT Model. *Phys. Chem. Chem. Phys.* **2016**, *18* (48), 32962−32972.

(7) Gulmen, T. S.; Thompson, W. H. Model Silica Pores with Controllable Surface Chemistry for Molecular Dynamics Simulations. *Mater. Res. Soc. Symp. Proc.* **2005**, *899*, N06-05.

(8) Ugliengo, P.; Sodupe, M.; Musso, F.; Bush, I. J.; Orlando, R.; Dovesi, R. Realistic Models of Hydroxylated Amorphous Silica Surfaces and MCM-41 Mesoporous Material Simulated by Large-scale Periodic B3LYP Calculations. *Adv. Mater.* **2008**, *20* (23), 4579−4583.

(9) Zhuravlev, L. T. The surface chemistry of amorphous silica. Zhuravlev model. *Colloids Surf., A* **2000**, *173* (1), 1−38.

(10) Morrow, B. A.; Gay, I. D. Silicon-29 cross-polarization/magic angle spinning NMR evidence for geminal silanols on vacuum-activated aerosil silica. *J. Phys. Chem.* **1988**, *92* (20), 5569−5571.

(11) Sindorf, D. W.; Maciel, G. E. Silicon-29 NMR study of dehydrated/rehydrated silica gel using cross polarization and magic-angle spinning. *J. Am. Chem. Soc.* **1983**, *105* (6), 1487−1493.

(12) Maciel, G. E.; Sindorf, D. W. Silicon-29 NMR study of the surface of silica gel by cross polarization and magic-angle spinning. *J. Am. Chem. Soc.* **1980**, *102* (25), 7606−7607.

(13) Van Roosmalen, A. J.; Mol, J. C. An infrared study of the silica gel surface. 1. Dry silica gel. *J. Phys. Chem.* **1978**, *82* (25), 2748−2751.

(14) McFarlan, A. J.; Morrow, B. A. Infrared evidence for two isolated silanol species on activated silicas. *J. Phys. Chem.* **1991**, *95* (14), 5388−5390.

(15) Williams, F. J.; Malikova, N.; Lambert, R. M. An AFM Study of the Genesis and Sintering in Hydrogen of a Realistic Cu/Amorphous Silica Planar Model Catalyst. *Catal. Lett.* **2003**, *90* (3), 177−180.

(16) Pfeiffer-Laplaud, M.; Costa, D.; Tielens, F.; Gaigeot, M.-P.; Sulpizi, M. Bimodal Acidity at the Amorphous Silica/Water Interface. *J. Phys. Chem. C* **2015**, *119* (49), 27354−27362.

(17) Leung, K.; Nielsen, I. M. B.; Criscenti, L. J. Elucidating the Bimodal Acid−Base Behavior of the Water−Silica Interface from First Principles. *J. Am. Chem. Soc.* **2009**, *131* (51), 18358−18365.

(18) Ong, S.; Zhao, X.; Eisenthal, K. B. Polarization of water molecules at a charged interface: second harmonic studies of the silica/water interface. *Chem. Phys. Lett.* **1992**, *191* (3), 327−335.

(19) Gierada, M.; De Proft, F.; Sulpizi, M.; Tielens, F. Understanding the Acidic Properties of the Amorphous Hydroxylated Silica Surface. *J. Phys. Chem. C* **2019**, *123* (28), 17343−17352.

(20) Macias-Romero, C.; Nahalka, I.; Okur, H. I.; Roke, S. Optical imaging of surface chemistry and dynamics in confinement. *Science* **2017**, *357* (6353), 784−788.

(21) Zheng, J.; Kwak, K.; Asbury, J.; Chen, X.; Piletic, I. R.; Fayer, M. D. Ultrafast Dynamics of Solute-Solvent Complexation Observed at Thermal Equilibrium in Real Time. *Science* **2005**, *309* (5739), 1338−1343.

(22) Kwak, K.; Zheng, J.; Cang, H.; Fayer, M. D. Ultrafast Two-Dimensional Infrared Vibrational Echo Chemical Exchange Experiments and Theory. *J. Phys. Chem. B* **2006**, *110* (40), 19998−20013.

(23) Fayer, M. D. Dynamics of liquids, molecules, and proteins measured with ultrafast 2D IR vibrational echo chemical exchange spectroscopy. *Annu. Rev. Phys. Chem.* **2009**, *60*, 21−38.

(24) Nishida, J.; Fayer, M. D. Guest Hydrogen Bond Dynamics and Interactions in the Metal−Organic Framework MIL-53(Al) Measured with Ultrafast Infrared Spectroscopy. *J. Phys. Chem. C* **2017**, *121* (21), 11880−11890.

(25) Dong, Y.; Pappu, S. V.; Xu, Z. Detection of Local Density Distribution of Isolated Silanol Groups on Planar Silica Surfaces Using Nonlinear Optical Molecular Probes. *Anal. Chem.* **1998**, *70* (22), 4730−4735.

(26) Fan, H.-F.; Li, F.; Zare, R. N.; Lin, K.-C. Characterization of Two Types of Silanol Groups on Fused-Silica Surfaces Using Evanescent-Wave Cavity Ring-Down Spectroscopy. *Anal. Chem.* **2007**, *79* (10), 3654−3661.

(27) Brunauer, S.; Emmett, P. H.; Teller, E. Adsorption of Gases in Multimolecular Layers. *J. Am. Chem. Soc.* **1938**, *60* (2), 309−319.

(28) Barrett, E. P.; Joyner, L. G.; Halenda, P. P. The Determination of Pore Volume and Area Distributions in Porous Substances. I. Computations from Nitrogen Isotherms. *J. Am. Chem. Soc.* **1951**, *73* (1), 373−380.
(29) Kruk, M.; Jaroniec, M.; Sayari, A. Adsorption Study of Surface and Structural Properties of MCM-41 Materials of Different Pore Sizes. *J. Phys. Chem. B* **1997**, *101* (4), 583−589.
(30) Kruk, M.; Jaroniec, M.; Sakamoto, Y.; Terasaki, O.; Ryoo, R.; Ko, C. H. Determination of Pore Size and Pore Wall Structure of MCM-41 by Using Nitrogen Adsorption, Transmission Electron Microscopy, and X-ray Diffraction. *J. Phys. Chem. B* **2000**, *104* (2), 292−301.
(31) Yamada, S. A.; Hung, S. T.; Thompson, W. H.; Fayer, M. D. Effects of pore size on water dynamics in mesoporous silica. *J. Chem. Phys.* **2020**, *152* (15), 154704.
(32) Karthick Kumar, S. K.; Tamimi, A.; Fayer, M. D. Comparisons of 2D IR measured spectral diffusion in rotating frames using pulse shaping and in the stationary frame using the standard method. *J. Chem. Phys.* **2012**, *137* (18), 184201.
(33) Yamada, S. A.; Shin, J. Y.; Thompson, W. H.; Fayer, M. D. Water Dynamics in Nanoporous Silica: Ultrafast Vibrational Spectroscopy and Molecular Dynamics Simulations. *J. Phys. Chem. C* **2019**, *123* (9), 5790−5803.
(34) Tan, H.-S.; Piletic, I. R.; Fayer, M. D. Polarization selective spectroscopy experiments: methodology and pitfalls. *J. Opt. Soc. Am. B* **2005**, *22* (9), 2009−2017.
(35) Hamm, P.; Zanni, M. T. *Concepts and Methods of 2D Infrared Spectroscopy*; Cambridge University Press: New York, 2011; p 286.
(36) Mukamel, S. *Principles of Nonlinear Optical Spectroscopy*; Oxford UP: New York, 1995.
(37) Park, S.; Kwak, K.; Fayer, M. D. Ultrafast 2D-IR vibrational echo spectroscopy: a probe of molecular dynamics. *Laser Phys. Lett.* **2007**, *4* (10), 704.
(38) Abelard, J.; Wilmsmeyer, A. R.; Edwards, A. C.; Gordon, W. O.; Durke, E. M.; Karwacki, C. J.; Troya, D.; Morris, J. R. Adsorption of Substituted Benzene Derivatives on Silica: Effects of Electron Withdrawing and Donating Groups. *J. Phys. Chem. C* **2016**, *120* (24), 13024−13031.
(39) Rimola, A.; Civalleri, B.; Ugliengo, P. Physisorption of aromatic organic contaminants at the surface of hydrophobic/hydrophilic silica geosorbents: a B3LYP-D modeling study. *Phys. Chem. Chem. Phys.* **2010**, *12* (24), 6357−6366.
(40) Thomas, G.; Eon, C. H. Adsorption from acetone, benzene, and carbon tetrachloride binary solutions on silica gel. *J. Colloid Interface Sci.* **1977**, *62* (2), 259−263.
(41) Everett, D. H. Thermodynamics of adsorption from solution. Part 1.—Perfect systems. *Trans. Faraday Soc.* **1964**, *60* (0), 1803−1813.
(42) Everett, D. Thermodynamics of adsorption from solution. Part 2.—Imperfect systems. *Trans. Faraday Soc.* **1965**, *61*, 2478−2495.
(43) Steinel, T.; Asbury, J. B.; Zheng, J.; Fayer, M. D. Watching Hydrogen Bonds Break: A Transient Absorption Study of Water. *J. Phys. Chem. A* **2004**, *108* (50), 10957−10964.
(44) Rezus, Y. L. A.; Bakker, H. J. On the orientational relaxation of HDO in liquid water. *J. Chem. Phys.* **2005**, *123* (11), 114502.
(45) Zheng, J.; Fayer, M. D. Solute−Solvent Complex Kinetics and Thermodynamics Probed by 2D-IR Vibrational Echo Chemical Exchange Spectroscopy. *J. Phys. Chem. B* **2008**, *112* (33), 10221−10227.
(46) Heilweil, E. J.; Casassa, M. P.; Cavanagh, R. R.; Stephenson, J. C. Population lifetimes of OH(v = 1) and OD(v = 1) stretching vibrations of alcohols and silanols in dilute solution. *J. Chem. Phys.* **1986**, *85* (9), 5004−5018.
(47) Casassa, M. P.; Heilweil, E. J.; Stephenson, J. C.; Cavanagh, R. R. Time-resolved measurements of OH(v = 1) vibrational relaxation on SiO_2 surfaces: Isotope and temperature dependence. *J. Chem. Phys.* **1986**, *84* (4), 2361−2364.
(48) Heilweil, E. J.; Casassa, M. P.; Cavanagh, R. R.; Stephenson, J. C. Vibrational deactivation of surface OH chemisorbed on SiO_2: Solvent effects. *J. Chem. Phys.* **1985**, *82* (11), 5216−5231.
(49) Mair, R. D.; Hornig, D. F. The Vibrational Spectra of Molecules and Complex Ions in Crystals. II. Benzene. *J. Chem. Phys.* **1949**, *17* (12), 1236−1247.
(50) Tokmakoff, A. Orientational correlation functions and polarization selectivity for nonlinear spectroscopy of isotropic media. I. Third order. *J. Chem. Phys.* **1996**, *105* (1), 1−12.
(51) Tao, T. Time-dependent fluorescence depolarization and Brownian rotational diffusion coefficients of macromolecules. *Biopolymers* **1969**, *8* (5), 609−632.
(52) Fecko, C. J.; Loparo, J. J.; Roberts, S. T.; Tokmakoff, A. Local hydrogen bonding dynamics and collective reorganization in water: Ultrafast infrared spectroscopy of HOD/D_2O. *J. Chem. Phys.* **2005**, *122* (5), 054506.
(53) Kramer, P. L.; Giammanco, C. H.; Fayer, M. D. Dynamics of water, methanol, and ethanol in a room temperature ionic liquid. *J. Chem. Phys.* **2015**, *142* (21), 212408.
(54) Tielens, F.; De Proft, F.; Geerlings, P. Density functional theory study of the conformation and energetics of silanol and disiloxane. *J. Mol. Struct.: THEOCHEM* **2001**, *542* (1), 227−237.
(55) Weinhold, F.; West, R. The Nature of the Silicon−Oxygen Bond. *Organometallics* **2011**, *30* (21), 5815−5824.
(56) Kinosita, K.; Kawato, S.; Ikegami, A. A theory of fluorescence polarization decay in membranes. *Biophys. J.* **1977**, *20* (3), 289−305.
(57) Lipari, G.; Szabo, A. Effect of librational motion on fluorescence depolarization and nuclear magnetic resonance relaxation in macromolecules and membranes. *Biophys. J.* **1980**, *30* (3), 489−506.
(58) Lipari, G.; Szabo, A. Model-free approach to the interpretation of nuclear magnetic resonance relaxation in macromolecules. 1. Theory and range of validity. *J. Am. Chem. Soc.* **1982**, *104* (17), 4546−4559.
(59) Moilanen, D. E.; Fenn, E. E.; Wong, D. B.; Fayer, M. D. Water Dynamics in Large and Small Reverse Micelles: From Two Ensembles to Collective Behavior. *J. Chem. Phys.* **2009**, *131*, 014704.
(60) Roget, S. A.; Kramer, P. L.; Thomaz, J. E.; Fayer, M. D. Bulk-like and Interfacial Water Dynamics in Nafion Fuel Cell Membranes Investigated with Ultrafast Nonlinear IR Spectroscopy. *J. Phys. Chem. B* **2019**, *123* (44), 9408−9417.
(61) Nishida, J.; Tamimi, A.; Fei, H.; Pullen, S.; Ott, S.; Cohen, S. M.; Fayer, M. D. Structural dynamics inside a functionalized metal−organic framework probed by ultrafast 2D IR spectroscopy. *Proc. Natl. Acad. Sci. U. S. A.* **2014**, *111* (52), 18442−18447.
(62) Cang, H. *Dynamics in Complex Liquids*; Stanford University: 2004.
(63) Ji, M.; Odelius, M.; Gaffney, K. J. Large Angular Jump Mechanism Observed for Hydrogen Bond Exchange in Aqueous Perchlorate Solution. *Science* **2010**, *328* (5981), 1003.
(64) Morrow, B. A.; McFarlan, A. J. Surface vibrational modes of silanol groups on silica. *J. Phys. Chem.* **1992**, *96* (3), 1395−1400.
(65) Fisk, J. D.; Batten, R.; Jones, G.; O'Reill, J. P.; Shaw, A. M. pH Dependence of the Crystal Violet Adsorption Isotherm at the Silica−Water Interface. *J. Phys. Chem. B* **2005**, *109* (30), 14475−14480.
(66) Morimoto, T.; Naono, H. The Heat of Adsorption from Solution. I. The Heat of Adsorption of Benzene on Silica Gel from the Benzene-Cyclohexane Solution. *Bull. Chem. Soc. Jpn.* **1972**, *45* (3), 700−705.
(67) Delle Piane, M.; Corno, M.; Ugliengo, P. Does Dispersion Dominate over H-Bonds in Drug−Surface Interactions? The Case of Silica-Based Materials As Excipients and Drug-Delivery Agents. *J. Chem. Theory Comput.* **2013**, *9* (5), 2404−2415.
(68) Hoffmann, P.; Knözinger, E. Novel aspects of mid and far IR Fourier spectroscopy applied to surface and adsorption studies on SiO_2. *Surf. Sci.* **1987**, *188* (1), 181−198.
(69) Sauer, J.; Schröder, K. P. Geminal Hydroxyls on Silica Surfaces and Their Role in Water Adsorption. *Z. Phys. Chem.* **1985**, *266* (1), 379−387.

https://doi.org/10.1021/acs.jpcb.1c01225
J. Phys. Chem. B 2021, 125, 4566−4581